2. EXPLANATORY NOTES[1]

Shipboard Scientific Party[2]

INTRODUCTION

Standard procedures for both drilling operations and preliminary shipboard analysis of the material recovered during Deep Sea Drilling Project (DSDP) and Ocean Drilling Program (ODP) drilling have been regularly amended and upgraded since drilling began in 1968. In this chapter, we have assembled information that will help the reader understand the basis for our preliminary conclusions and also help the interested investigator select samples for further analysis. This information concerns only shipboard operations and analyses described in the site reports in the *Initial Reports* volume of the Leg 135 *Proceedings of the Ocean Drilling Program*. Methods used by various investigators for shore-based analysis of Leg 135 data will be detailed in the individual scientific contributions published in the *Scientific Results* volume.

Authorship of Site Chapters

The separate sections of the site chapters were written by the following shipboard scientists (authors are listed in alphabetical order; no seniority is implied):

Site Summary: Hawkins, Parson
Background and Objectives: Hawkins, Parson
Operations: Allan, Hawkins, Parson, Pollard
Lithostratigraphy: Bednarz, Bøe, Clift, Hodkinson, Ledbetter, Pratt, Rothwell, Soakai
Structural Geology: MacLeod
Biostratigraphy: Chaproniere, Nishi, Quinterno, Styzen
Sediment Accumulation Rates: Chaproniere
Paleomagnetics: Abrahamsen, Sager
Inorganic Geochemistry: Blanc
Organic Geochemistry: Fowler
Igneous Petrology: Allan, Bloomer, Bryan, Ewart, Hawkins, Hergt, Nilsson, Schöps
Physical Properties: Bruns, LaVoie
Downhole Measurements: Bruns, LaVoie, MacLeod, Reynolds, Schwarz
Discussion: Hawkins, Parson
Appendix: Shipboard Scientific Party

Corresponding with the text of each site chapter are summary core descriptions ("barrel sheets" and igneous rock visual core descriptions) and photographs of each core.

Survey and Drilling Data

The geophysical survey data collected during Leg 135 fall into two categories: (1) magnetic, seismic reflection profile, and bathymetric data acquired during site surveys immediately before drilling and (2) a more comprehensive set of seismic data collected around Site 840 as required by the Pollution Prevention and Safety Panel. The survey data used for final site selection, including both data collected during site surveys before Leg 135 and on short site-location surveys during Leg 135, are presented in the "Background and Objectives" section of the individual site chapters (this volume). During the Leg 135 *JOIDES Resolution* surveys, single-channel seismic and 3.5- and 12-kHz echo sounder, in addition to magnetic, data were recorded across the planned drilling sites to aid site confirmation before dropping the location beacon.

The single-channel seismic profiling system used two 80-in.^{3} water guns as the energy source and a Teledyne streamer with a 100-m-long active section. These data were recorded digitally on tape using a Masscomp 561 super minicomputer and were also displayed in real time in analog format on two Raytheon recorders using a variety of filter settings (commonly 30–150 Hz) and various vertical scales, dependant on the water depth.

Bathymetric data collected using the 3.5- and 12-kHz Precision Depth Recorder (PDR) systems were displayed on two Raytheon recorders. The depths were calculated on the basis of an assumed 1463 m/s sound velocity in water. The water depth (in meters) at each site was corrected for (1) the variation in sound velocity with depth using Matthews' (1939) tables and (2) the depth of the transducer pod (6.8 m) below sea level. In addition, depths referred to the drilling-platform level are corrected for the height of the rig floor above the water line, which gradually increased from 10.6 to 11.2 m throughout the cruise (see Fig. 1).

Magnetic data were collected using a Geometrics 801 proton precession magnetometer, displayed on a strip chart recorder, and recorded on magnetic tape for later processing.

Drilling Characteristics

Because the water circulation downhole is open, cuttings are lost onto the seafloor and cannot be examined. Information concerning sedimentary stratification in uncored or unrecovered intervals may be inferred from seismic data, wireline-logging results, and an examination of the behavior of the drill string as observed and recorded on the drilling platform. Typically, the harder a layer, the slower and more difficult it is to penetrate. A number of other factors may determine the rate of penetration, so it is not always possible to relate the drilling time directly to the hardness of the layers. Bit weight and revolutions per minute, recorded on the drilling recorder, also influence the penetration rate.

Drilling Deformation

When cores are split, many show signs of significant sediment disturbance, including the concave-downward appearance of originally horizontal bands, haphazard mixing of lumps of different lithologies (mainly at the tops of cores), and the near-fluid state of some sediments recovered from tens to hundreds of meters below the seafloor. Core deformation probably occurs during cutting, retrieval (with accompanying changes in pressure and temperature), and core handling on deck.

---

[1] Parson, L., Hawkins, J., Allan, J., et al., 1992. *Proc. ODP, Init. Repts.*, 135: Ocean Drilling Program (College Station, TX).

[2] Shipboard Scientific Party is as given in the list of participants preceding the contents.

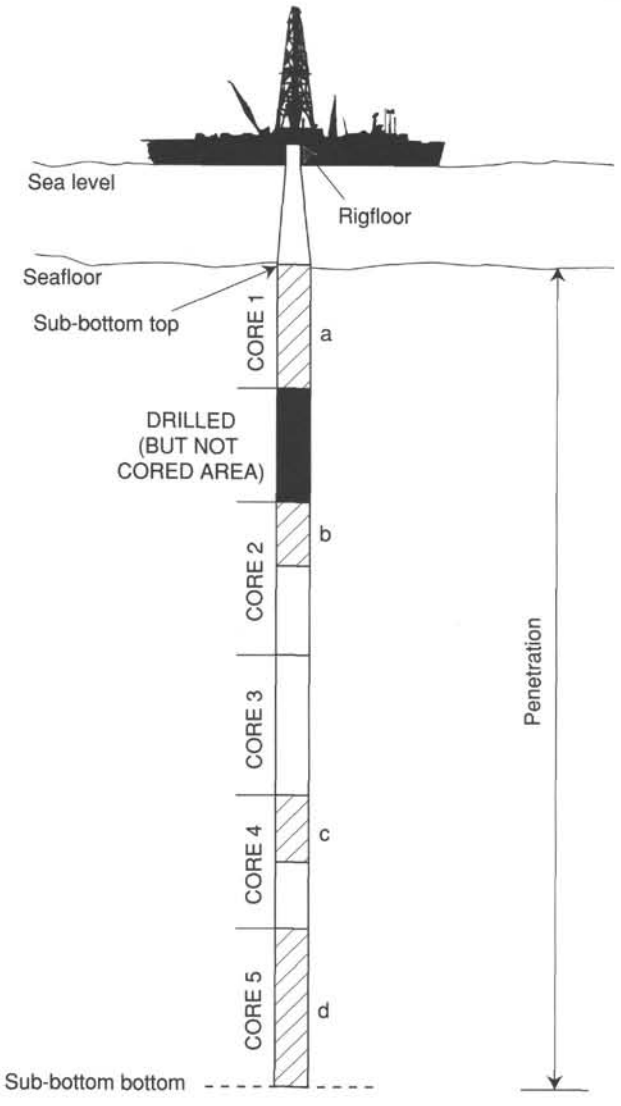

Represents recovered material

BOTTOM FELT: distance from rig floor to seafloor

TOTAL DEPTH: distance from rig floor to bottom of hole (sub-bottom bottom)

PENETRATION: distance from seafloor to bottom of hole (sub-bottom bottom)

NUMBER OF CORES: total of all cores recorded, including cores with no recovery

TOTAL LENGTH OF CORED SECTION: distance from sub-bottom top to sub-bottom bottom minus drilled (but not cored) areas in between

TOTAL CORE RECOVERED: total from adding a, b, c, and d in diagram

CORE RECOVERY (%): equals TOTAL CORE RECOVERED divided by TOTAL LENGTH OF CORED SECTION times 100

Figure 1. Diagram illustrating terms used in the discussion of coring operations and core recovery.

SHIPBOARD SCIENTIFIC PROCEDURES

Numbering of Sites, Holes, Cores, and Samples

Drilling sites are numbered consecutively from the first site drilled by the *Glomar Challenger* in 1968. A site number is used for one or more holes drilled while the ship was positioned over one acoustic beacon. Multiple holes may be drilled at a single site by pulling the drill pipe above the seafloor (out of the hole), moving the ship some distance from the previous hole, and then drilling another hole. In some cases, the ship may return to a previously occupied site to drill additional holes.

For all ODP drill sites, a letter suffix distinguishes each hole drilled at the same site. For example, the first hole drilled is assigned the site number modified by the suffix *A*, the second hole takes the site number and the suffix *B*, and so forth. Note that this procedure differs slightly from that used by DSDP (Sites 1 through 624), but prevents ambiguity between site- and hole-number designations. It is important to distinguish among holes drilled at a site, because recovered sediments or rocks from different holes usually do not come from equivalent positions in the stratigraphic column.

The cored interval is measured in meters below seafloor (mbsf); sub-bottom depths are determined by subtracting the drill pipe measurement (DPM) water depth (the length of pipe from the rig floor to the seafloor) from the total DPM (from the rig floor to the bottom of the hole; see Fig. 1). Note that although the echo-sounding data (from the PDR systems) are used to locate the site, they are not used as a basis for further measurements.

The depth interval assigned to an individual core begins with the depth below the seafloor that the coring operation began and extends to the depth that the coring operation ended for that core (see Fig. 1). For rotary coring (RCB and XCB), each coring interval is equal to the length of the joint of drill pipe added for that interval (though a shorter core may be attempted in special instances). The drill pipe in use varies from about 9.4 to 9.8 m. The pipe is measured as it is added to the drill string, and the cored interval is recorded as the length of the pipe joint to the nearest 0.1 m. For hydraulic piston coring (APC) operations, the drill string is advanced 9.5 m, the maximum length of the piston stroke.

Coring intervals may be shorter and are not necessarily adjacent, but may be separated by drilled intervals. In soft sediments, the drill string can be "washed ahead" with the core barrel in place, without recovering sediments. This is achieved by pumping water down the pipe at high pressure to wash the sediment out of the way of the bit and up the annulus between the drill pipe and the wall of the hole. If thin, hard, rock layers are present, then it is possible to get "spotty" sampling of these resistant layers within the washed interval, and thus have a cored interval greater than 9.5 m. In drilling hard rock, a center bit may replace the core barrel if it is necessary to drill without core recovery.

Cores taken from a hole are numbered serially from the top of the hole downward. Core numbers and their associated cored intervals (in mbsf) usually are unique in a given hole; however, this may not be true if an interval must be cored twice, because of caving of cuttings or other hole problems. Maximum full recovery for a single core is 9.5 m of rock or sediment contained in a plastic liner (6.6-cm internal diameter) plus about 0.2 m (without a plastic liner) in the core catcher (Fig. 2). The core catcher is a device at the bottom of the core barrel that prevents the core from sliding out when the barrel is being retrieved from the hole. For sediments, the core-catcher sample is extruded into a short piece of plastic liner and is treated as a separate section below the last core section. For hard rocks, material recovered in the core catcher is included at the bottom of the last section. In certain situations (e.g., when coring gas-charged sediments that expand while being brought on deck), recovery may exceed the 9.5-m maximum.

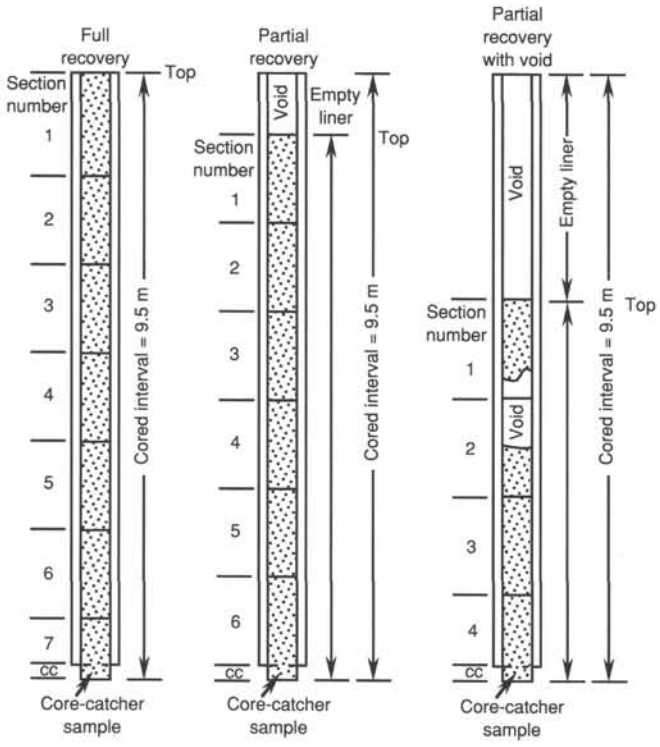

Figure 2. Diagram showing the procedure used in cutting and labeling recovered core sections.

A recovered core is divided into 1.5-m sections that are numbered serially from the top (Fig. 2). When full recovery is obtained, the sections are numbered from 1 through 7, with the last section possibly being shorter than 1.5 m (rarely, an unusually long core may require more than seven sections). When less than full recovery is obtained, there will be as many sections as needed to accommodate the length of the core recovered; for example, 4 m of core would be divided into two 1.5-m sections and one 1-m section. If cores are fragmented (recovery less than 100%), sections are numbered serially and intervening sections are noted as void, whether shipboard scientists think that the fragments were contiguous *in situ* or not. In rare cases, a section <1.5 m may be cut to preserve features of interest (e.g., lithologic contacts).

By convention, material recovered from the core catcher is placed below the last section when the core is described, and labeled core catcher (CC). The core catcher is placed at the top of the cored interval in cases where material is recovered only in the core catcher. However, information supplied by the drillers or other sources may allow for more precise interpretation as to the correct position of core-catcher material within an incompletely recovered cored interval.

Igneous rock cores are also cut into 1.5-m sections that are numbered serially; individual pieces of rock are then each assigned a number. Fragments of a single piece are assigned a single number, and individual fragments are identified alphabetically. The core-catcher sample is treated as part of the last section, rather than separately. Scientists completing visual core descriptions describe each lithologic unit, noting core and section boundaries only as physical reference points.

When, as is usually the case, the recovered core is shorter than the cored interval, the top of the core is equated with the top of the cored interval by convention, in order to achieve consistency in handling analytical data derived from the cores. Samples removed from the cores are designated by the distance measured in centimeters from the top of the section to the top and bottom of each sample removed from that section. In curated hard-rock sections, sturdy plastic spacers are placed between pieces that do not fit together in order to protect them from damage in transit and in storage; therefore, the centimeter interval noted for a hard-rock sample has no direct relationship to that sample's depth within the cored interval, but is only a physical reference to the location of the sample within the curated core.

A full identification number for a sample consists of the following information: leg, site, hole, core number and type, section number, piece number (for hard rock), and interval in centimeters measured from the top of section. For example, a sample identification of "135-835A-5H-1, 10–12 cm" would be interpreted as representing a sample removed from the interval between 10 and 12 cm below the top of Section 1, Core 5 (H designates that this core was taken during hydraulic piston coring) of Hole 835A during Leg 135.

All ODP core and sample identifiers indicate core type. The following abbreviations are used: R = rotary core barrel (RCB); H = hydraulic piston core (HPC; also referred to as APC, or advanced hydraulic piston core); P = pressure core sampler; X = extended core barrel (XCB); B = drill-bit recovery; C = center-bit recovery; I = *in situ* water sample; S = sidewall sample; W = wash-core recovery; and M = miscellaneous material. APC, XCB, RCB, M, and W cores were collected on Leg 135.

CORE HANDLING

Sediments

As soon as a core was retrieved on deck, a sample was taken from the core catcher and given to the paleontological laboratory for an initial age assessment. The core was then placed on the long horizontal rack, and any gas samples were taken by piercing the core liner and withdrawing gas into a vacuum tube. Voids within the core were sought as sites for gas sampling. Some of the gas samples were stored for shore-based study, but others were analyzed immediately as part of the shipboard safety and pollution-prevention program. Next, the core was marked into section lengths, each section was labeled, and the core was cut into sections. Interstitial-water (I) samples were then taken. In addition, some headspace gas samples were scraped from the ends of sections immediately after cutting, and sealed in glass vials for light hydrocarbon analysis. Each section was then sealed at the top and bottom by gluing on color-coded plastic caps: blue to identify the top of a section and clear for the bottom. A yellow cap was placed on a section end from which a whole-round sample had been removed, and the sample code (e.g., I) was written on the cap. The caps were usually attached to the liner by coating the end of the liner and the inside rim of the cap with acetone and then taping the caps to the liners.

The cores were then carried into the laboratory, where the sections were labeled again, using an engraver to permanently mark the full designation of the section. The length of the core in each section and the core-catcher sample were measured to the nearest centimeter; this information was logged in the shipboard CORELOG database program.

Whole-round sections from APC and XCB cores were normally run through the multisensor track (MST). The MST includes the gamma-ray attenuation porosity evaluator (GRAPE) and *P*-wave logger devices, which measure bulk density, porosity, and sonic velocity; it also includes a meter that determines the volume magnetic susceptibility. At this point, whole-round samples for physical properties (P) and structural analysis were taken. In well-lithified sedimentary cores, the core liner was split and the top half removed so that the whole-round core could be observed before choosing the samples. Relatively soft sedimentary cores were equilibrated to room temperature (approximately

3 hr) and thermal-conductivity measurements were performed on them.

Cores of soft material were split lengthwise into working and archive halves. The softer cores were split with a wire or saw, depending on the degree of induration. Harder cores were split with a band saw or diamond saw. The wire-cut cores were split from bottom to top, so investigators should be aware that older material could have been transported up the core on the split face of each section.

The working half of each core was sampled for both shipboard and shore-based laboratory studies. Each extracted sample was logged in the computerized sample database program by location and the name of the investigator receiving the sample. Records of all removed samples are kept by the Curator at ODP headquarters. The extracted samples were sealed in plastic vials or bags and labeled. The samples taken routinely for shipboard physical-property analysis were subsequently used for calcium carbonate (coulometric analysis) and organic carbon (CNS elemental analyzer); the data are reported in the site chapters.

The archive half was used for the visual core description. The smear slides made from samples taken from the archive half are supplemented by thin sections taken from the working half. Most of the archive sections were run through the cryogenic magnetometer. The archive half was then photographed with both black-and-white and color film, a whole core at a time. Close-up photographs (black-and-white) were taken of particular features, as requested by individual scientists.

Both halves of the core were then put into labeled plastic tubes, sealed, and transferred to cold-storage space aboard the drilling vessel. At the end of Leg 135, the cores were transferred from the ship in refrigerated air freight containers to cold storage at the Gulf Coast ODP Repository, Texas A&M University, College Station, Texas.

Igneous and Metamorphic Rocks

Igneous and metamorphic rock cores were handled differently from the sedimentary cores. Once on deck, the core-catcher recovery was placed at the bottom of the core liner and the total core recovery was calculated by shunting the rock pieces together and measuring to the nearest centimeter; this information was logged in the shipboard CORELOG database program. The core was then cut into 1.5-m-long sections and carried into the laboratory.

The contents of each section were transferred into 1.5-m-long sections of split core liner, and the bottom of each oriented piece (i.e., a piece that clearly could not have rotated top to bottom about a horizontal axis in the liner) was marked with a red wax pencil. This was to ensure that the orientation was not lost during the splitting and labeling process. Pieces were grouped together where it could be established that they were originally continuous. The core was then split into archive and working halves. A plastic spacer was used to separate individual pieces and/or reconstructed groups of pieces in the core liner. These spacers may represent a substantial interval of no recovery. Each piece was numbered sequentially from the top of each section, beginning with the number 1; reconstructed groups of pieces were assigned the same number, but were also lettered consecutively. Pieces were labeled only on external surfaces. If the piece was oriented, an arrow was added to the label pointing to the top of the section.

The working half of the hard-rock core was then sampled for shipboard laboratory studies. Records of all samples are kept by the Curator at ODP headquarters.

The archive half was used for the visual core description, and then photographed with both black-and-white and color film, one core at a time. Both halves of the core were then shrink-wrapped in plastic to prevent the rock pieces from vibrating out of sequence during transit, put into labeled plastic tubes, sealed, and transferred to cold-storage space aboard the drilling vessel. As for the other Leg 135 cores, they are housed in the Gulf Coast ODP Repository.

SEDIMENT CORE DESCRIPTION FORMS

The sediment core description forms (Fig. 3), or barrel sheets, summarize the sedimentological data obtained during the shipboard analysis of each sediment core. The following discussion explains the ODP conventions used in compiling each part of the core description forms and the modifications of these procedures adopted by the Leg 135 scientists. The barrel sheets produced for Leg 135 differ from those produced on previous ODP legs, principally by omitting paleontological, geochemical, paleomagnetic, and physical properties data. The barrel sheets for each core are included in the Appendix.

Core Designation

The cores are designated using leg, site, hole, core number, and core type as previously discussed (see "Numbering of Sites, Holes, Cores, and Samples" section, this chapter). In addition, the cored interval is specified in terms of meters below sea level (mbsl) and meters below seafloor. On Leg 135, these depths were based on the DPM, as reported by the SEDCO coring technician and the ODP operations superintendent.

Graphic Lithology Column

The lithological classification scheme of Mazzullo et al. (1987), accepted for shipboard use by the JOIDES Sediments and Ocean History Panel, was slightly modified for use on Leg 135. The classification adopted is outlined in the "Classification of Sediments and Sedimentary Rocks" section of this chapter. The only significant modification is in the division of volcaniclastic sediment into two types: *pyroclastic* and *epiclastic* with the subdivision of pyroclastic sediment into *fine ash* and *coarse ash*. *Fine ash* and *coarse ash* are represented by different symbols on the core description forms but no new symbol is introduced for epiclastic volcaniclastic sediments. Instead, the symbolic designation for epiclastic sediments on the core description form is the same as the textural terms used for siliciclastic rocks (sand, silt, etc.) but differentiation is made by using the modifier *volcanic* before the principal name (e.g., volcanic silt, volcanic sand). Sediment type is represented graphically on the core description forms using the symbols illustrated in Figure 4.

In the "Graphic Lithology" column, a maximum of three different lithologies can be represented within the same interval of core. Percentages are rounded to the nearest 10% and only lithologies that constitute at least 10% of the core are shown. Only lithologic units that are 16 cm or greater in thickness are represented. Minor components may be present either as thin interbeds within the major lithology (shown by a dashed vertical line dividing the lithologies) or as a minor fraction of the main lithology (shown by a continuous vertical line).

Some cores recovered during Leg 135 have intercalations of sedimentary material located between lava flows or intrusive sills. Intervals described by igneous petrologists are indicated by the appropriate symbols for the igneous rocks cored (see the "Visual Core Description Forms" section that corresponds with this chapter).

Age

The chronostratigraphic unit, determined by micropaleontological and paleomagnetic criteria, is shown in the "Age" column. Shipboard paleontologists generally base their age determinations on core-catcher samples, although additional samples from other parts of the core may be examined when required. Boundaries are

Smear Slide and thin section summary (%)
Section, depth (cm)
M = minor litholgy
D = dominant lithology

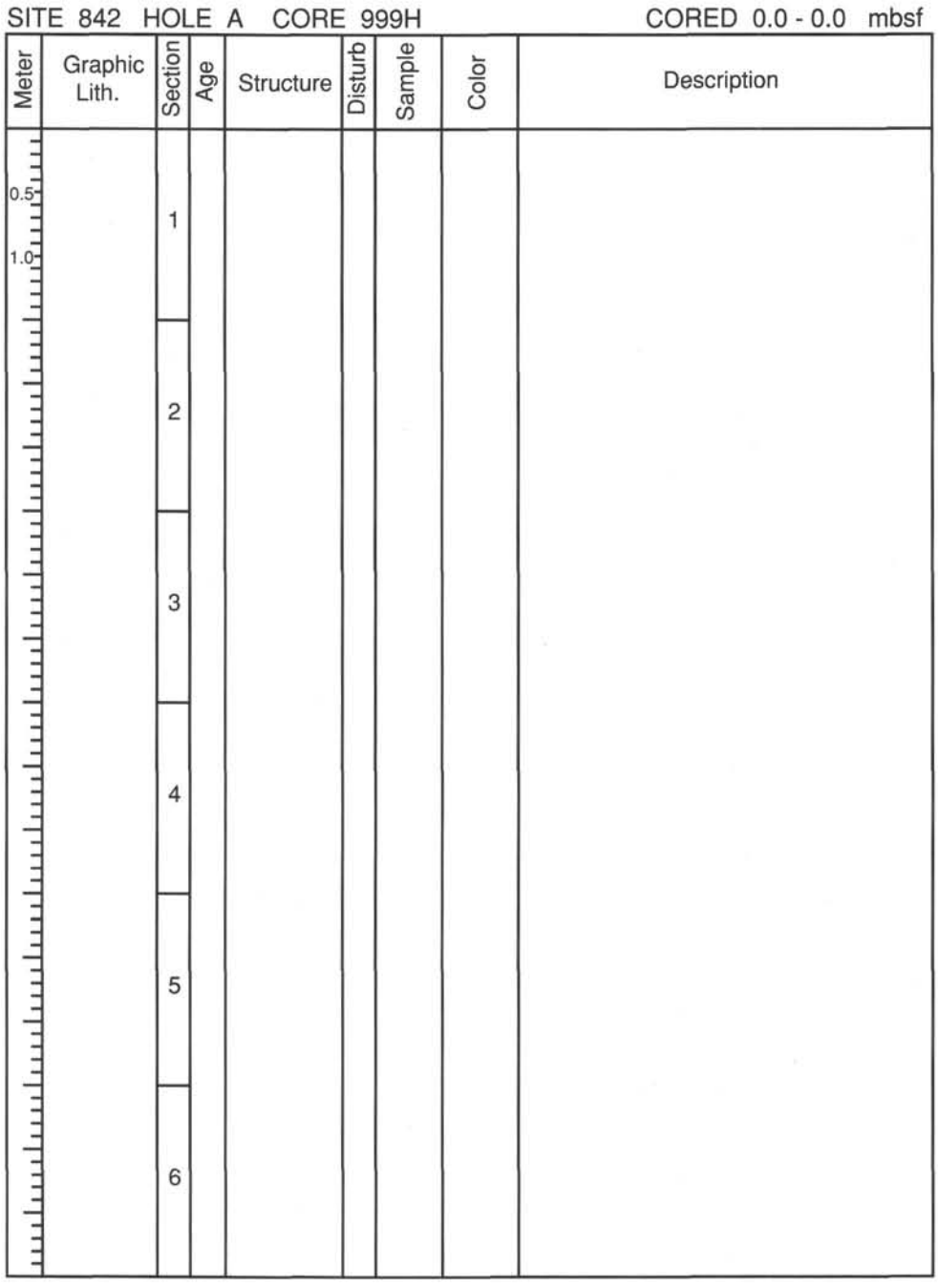

Figure 3. Core description form (barrel sheet) used for sediments and sedimentary rocks.

shown for the ages indicated on the core description forms by the following:

1. sharp = straight line;
2. unconformity or hiatus = wavy line;
3. uncertain = ? (question mark).

Sedimentary Structures

Sedimentary structures are indicated in the "Structure" column of the core description forms. A key to the structural symbols used on Leg 135 is given in Figure 5. It should be noted that on Leg 135, the descriptive terms *mottled* and *strongly mottled* were used instead of the more genetic terms *bioturbated* and *strongly bioturbated*. The term *mottled* may indicate the presence of burrows or other penecontemporaneous or postdepositional changes to the sediment, including chemical haloes and other diagenetic effects. Original sedimentary structures may have been destroyed in cores that have been severely disturbed by drilling.

Sediment Disturbance

The coring techniques used may result in varying degrees of disturbance of the recovered core material. Observations of drilling-related disturbance over an interval of 20 cm or more are recorded in the "Disturbance" column on the core description form. The symbols for the various types of drilling disturbance are shown in Figure 5.

The following disturbance categories are recognized for unlithified and partially lithified sediments:

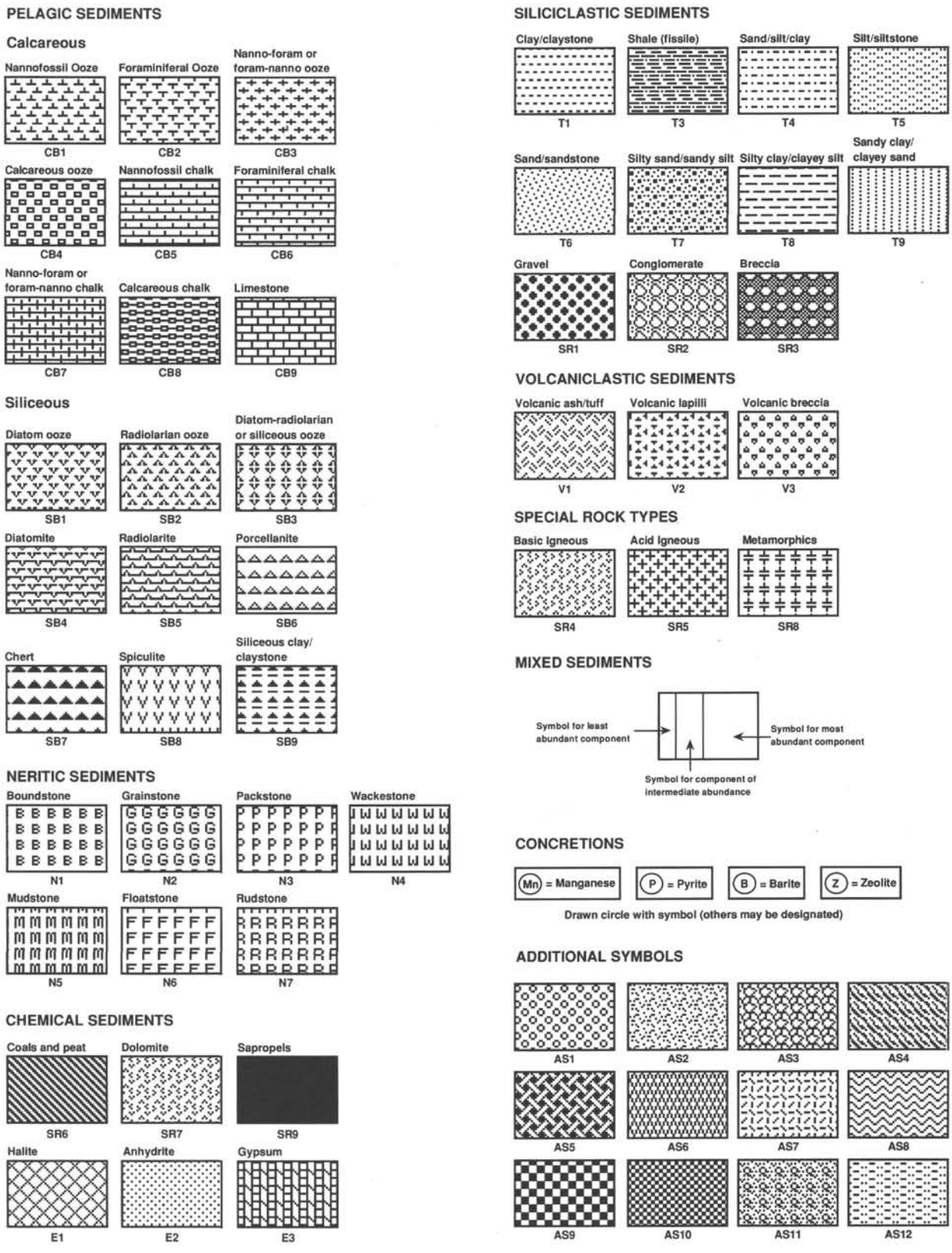

Figure 4. Key to symbols used in the "Graphic Lith." column on the core description form shown in Figure 3.

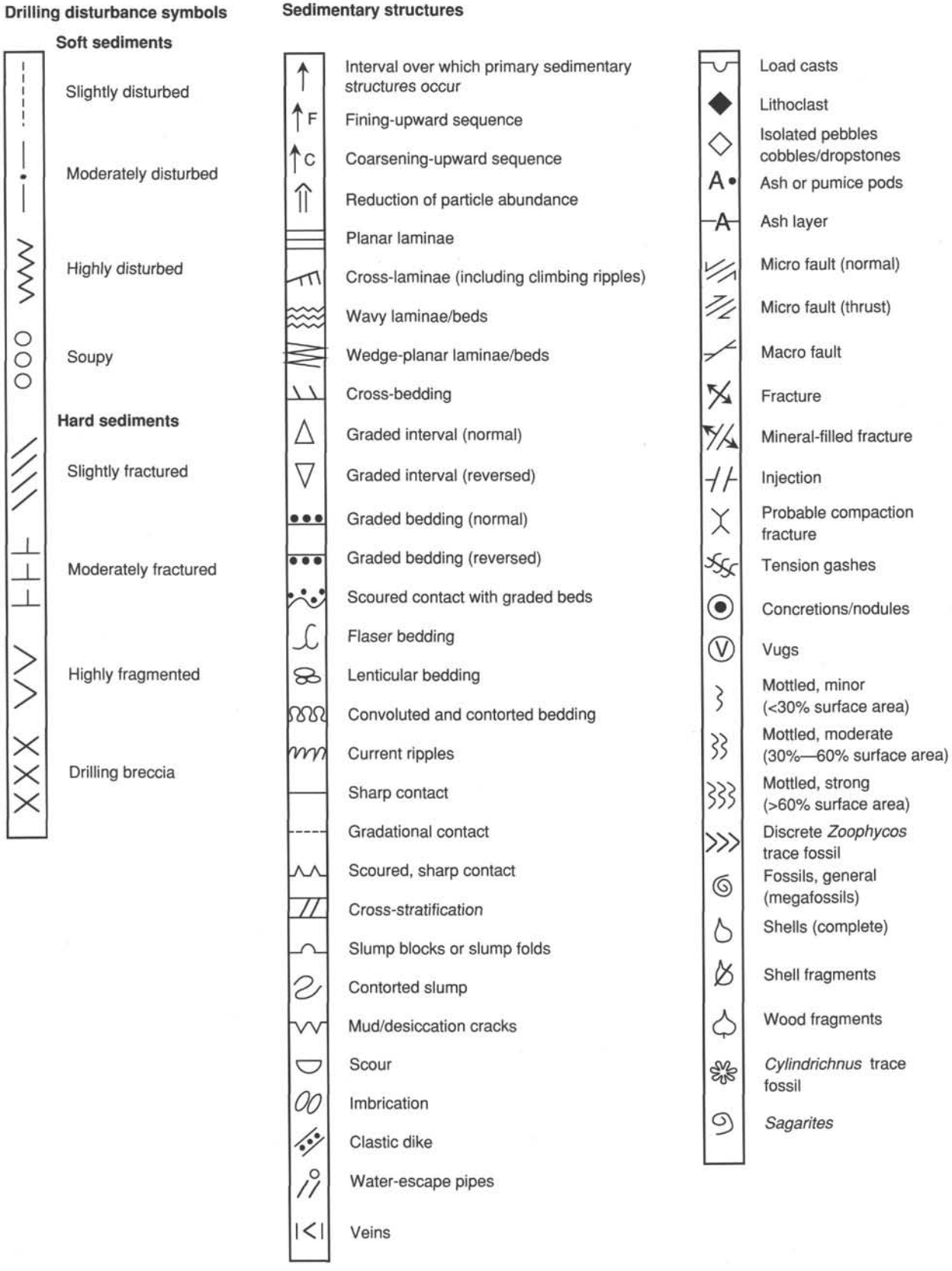

Figure 5. Symbols used for drilling disturbance and sedimentary structures on core description form shown in Figure 3.

1. Slightly deformed: bedding contacts are slightly bowed toward their edges.
2. Moderately deformed: bedding contacts have undergone extreme bowing.
3. Highly deformed: bedding is completely disturbed, and some shows symmetrical diapirlike structures ("flow-in").
4. Soupy: intervals are water-saturated and have lost all traces of original bedding.

The following categories are used to describe the degree of fracturing in lithified sediments and igneous rocks:

1. Slightly fractured: core pieces are in place and have very little drilling slurry or breccia.
2. Moderately fragmented: core pieces are in place or partly displaced, but original orientation is preserved or recognizable. Drilling slurry may surround fragments.
3. Highly fragmented: pieces are from the interval cored and probably in correct stratigraphic sequence (although they may not represent the entire section), but the original orientation is totally lost.
4. Drilling breccia: core pieces have completely lost their original orientation and stratigraphic position and may be completely mixed with drilling slurry.

Samples

The positions of samples taken from each core for analysis are indicated by letters in the "Sample" column of the core description form, as follows:

S: smear slide
T: thin section
P: physical properties sample
M: micropaleontology sample
X: paleomagnetic sample
I: interstitial-water sample
C: organic geochemistry sample
D: XRD sample
F: XRF sample

Smear Slide Summary

A table summarizing data from smear slides and thin sections appears on each core barrel description form. These tables include information about the sample location (by section number and centimeter interval) above each column (see first barrel sheet for further clarification); whether the sample represents a dominant (D) or a minor (M) lithology in the core; and the estimated percentage ranges of sand, silt, and clay, together with all identified components. Smear slide analyses provide only crude estimates of the relative abundances of detrital constituents; the mineralogies of finer grained particles are difficult to identify petrographically, and sand-sized grains tend to be underestimated because they cannot be incorporated into the smear evenly. In addition, estimates of grain size suffer from systematic errors because of differences between the surface areas of grains and their respective weight-percentages; this is particularly problematic with clay-sized particles. Coarse-fraction separates were made of selected samples and the wt% > 63 µm was reported on the barrel sheets as "Percent Sand."

Color

Colors of sediment are determined by comparison with the Munsell Soil Color Charts (1975). This was done immediately after the cores were split and while they were still wet, to minimize alteration caused by exposure to air. Colors of the indurated sediments were determined from wet samples. Color, hue, and chroma codes are shown in the "Color" column of the core description form. Intervals of 34 cm or greater are represented by a single color code. Intervals of 80 cm or greater are represented by two color codes, indicating either two colors or a gradation between two colors. The color of thinner units (less than 34 cm) may be given in the "Description" column.

Lithologic Description

The lithologic description that appears on each core description form consists of a brief summary of the major lithologies observed, followed by a summary of the minor lithologies. The color, composition (determined from the analysis of smear slides), sedimentary structures, or other notable features of each lithology are described and, where possible, the distribution of these features in the core is indicated.

The thickness of sedimentary beds and laminae is described using the terminology of McKee and Weir (1953): very thick bedded (>100 cm thick), thick bedded (30–100 cm thick), medium bedded (10–30 cm thick), thin bedded (3–10 cm thick), and very thin bedded (1–3 cm thick). Some beds of medium thickness and all thin or very thin beds of a minor lithology may be described in the "Description" column, although the beds may be too thin (<16 cm) to appear in the "Graphic Lithology" column. Additional data collected during Leg 135 (e.g., grain-size, wireline log, paleomagnetic, geochemical, micropaleontological, and physical-property data) can be plotted as downcore profiles in the two columns to the left of the meter scale on the core description form (Fig. 3).

CLASSIFICATION OF SEDIMENTS AND SEDIMENTARY ROCKS

Leg 135 used a slightly modified version of the ODP sediment classification scheme (Mazzullo et al., 1987), which defines (1) *granular* and (2) *chemical* sediment types. *Granular* sediments consist of discrete organic (e.g., foraminifer tests, mollusk shells) or inorganic (e.g., quartz grains, rock fragments, volcanic ash) grains. Some examples of granular sediment are foraminiferal chalk, quartz sandstone, fine vitric ash, and bioclastic grainstone. *Chemical* sediments consist of minerals formed by inorganic processes, such as precipitation from solution or colloidal suspension, deposition of insoluble precipitates, or recrystallization of detrital grains. Some examples of chemical sediments are coal, halite, pyrite, and gypsum.

The ODP sediment classification scheme (Mazzullo et al., 1987) is reproduced in the following. However, we modified the classification by dividing volcaniclastic sediment into two types: *pyroclastic* and *epiclastic*.

Granular Sediments

Classes of Granular Sediments

Variations in the relative proportions of pelagic, neritic, siliciclastic, and volcaniclastic grain types define five major classes of granular sediments: *pelagic, neritic, siliciclastic, volcaniclastic,* and *mixed* (Fig. 6). *Pelagic* grains are the skeletal remains of open-marine siliceous and calcareous microfauna and microflora (e.g., radiolarians, planktonic foraminifers, nannofossils) and associated organisms. *Neritic* grains include calcareous grains and skeletal remains (e.g., bioclasts, shallow-water benthic foraminifers, peloids) of nonpelagic origin. *Siliciclastic* grains are mineral and rock fragments derived from plutonic, sedimentary, and metamorphic rocks. *Volcaniclastic* grains include those of pyroclastic (direct products of magma degassing) and epiclastic (detritus derived from erosion of volcanic rocks) origins.

Pelagic sediments are composed of >60% pelagic and neritic grains and <40% siliciclastic and volcaniclastic grains, and con-

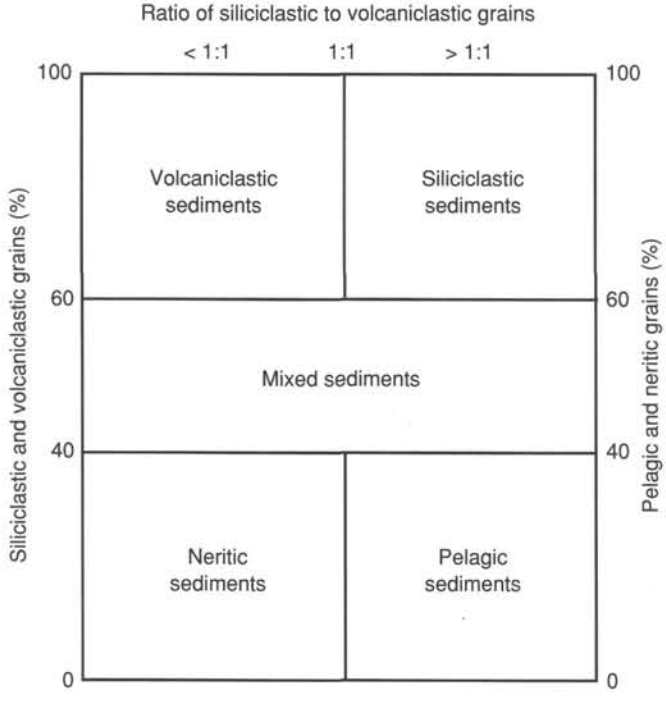

Figure 6. Diagram showing classes of granular sediment (modified from Mazzullo et al., 1987).

tain a higher proportion of pelagic than neritic grains (Fig. 6). *Neritic* sediments are composed of >60% pelagic and neritic grains and <40% siliciclastic and volcaniclastic grains, but contain a higher proportion of neritic than pelagic grains. *Siliciclastic* sediments are composed of >60% siliciclastic and volcaniclastic grains and <40% pelagic and neritic grains, with a higher proportion of siliciclastic than volcaniclastic grains. *Volcaniclastic* sediments are composed of >60% siliciclastic and volcaniclastic grains and <40% pelagic and neritic grains, with a higher proportion of volcaniclastic than siliciclastic grains. *Mixed* sediments are composed of 40% to 60% siliciclastic and volcaniclastic grains, and 40% to 60% pelagic and neritic grains.

Classification of Granular Sediment

A granular sediment is classified by designating a principal name with additional major and minor modifiers. The principal name of a granular sediment defines its granular-sediment class. The major and minor modifiers describe the texture, composition, fabric, or roundness of the grains themselves (Table 1).

Principal Names

Each granular sediment class has a unique set of principal names. A summary of these principal names is presented in the following.

Pelagic Sediment. For pelagic sediment, the principal name describes the composition and degree of induration using the following terms:

Table 1. Outline of granular-sediment classification scheme (modified from Mazzullo et al., 1987).

Sediment class	Major modifiers	Principal name	Minor modifiers
Pelagic sediment	Composition of pelagic and neritic grains present in major amounts Texture of clastic grains present in major amounts	Ooze Chalk Limestone Radiolarite Diatomite Spiculite Chert	Composition of pelagic and neritic grains present in minor amounts Texture of clastic grains present in minor amounts
Neritic sediment	Composition of neritic and pelagic grains present in major amounts Texture of clastic grains present in major amounts Degree of lithification	Boundstone Grainstone Packstone Wackestone Mudstone Floatstone Rudstone	Composition of neritic and pelagic grains present in minor amounts Texture of clastic grains present in minor amounts
Siliciclastic sediment	Composition of all grains present in major amounts Grain fabric (gravels only) Grain shape (optional) Sediment color (optional) Degree of lithification (optional)	Gravel, breccia, Conglomerate Sand Silt Clay	Composition of all grains present in minor amounts Texture and composition of siliciclastic grains present as matrix (for coarse-grained clastic)
Volcaniclastic sediment	Composition of all grains present in major amounts Texture of clastic grains present in major amounts Degree of lithification (optional)	Pyroclastic: Volcanic breccia Lapilli Coarse ash/tuff Fine ash/tuff Epiclastic: Volcanic Conglomerate Ig-lithic breccia Volcanic sand Volcanic silt	Composition of all volcaniclasts present in minor amounts Composition of all neritic and pelagic grains present in minor amounts Texture of clastic grains present in minor amounts
Mixed sediments	Composition of neritic and pelagic grains present in major amounts Texture of clastic grains present in major amounts	Mixed sediments/ mixed sedimentary rock	Composition of neritic and pelagic grains present in minor amounts Texture of clastic grains present in minor amounts

1. *Ooze:* unlithified calcareous and/or siliceous pelagic sediments;
2. *Chalk:* partially lithified pelagic sediment composed predominantly of calcareous pelagic grains;
3. *Limestone:* lithified pelagic sediment composed predominantly of calcareous pelagic grains;
4. *Radiolarite, diatomite,* and *spiculite:* partially lithified pelagic sediment composed predominantly of siliceous radiolarians, diatoms, and sponge spicules, respectively;
5. *Chert:* lithified pelagic sediment composed predominantly of siliceous pelagic grains.

Neritic Sediment. For neritic sediment, the principal name describes the texture and fabric using the following terms (after Dunham, 1962; Embry and Klovan, 1971). Note that the suffix *-stone* does not signify lithification.

1. *Boundstone:* components organically bound during deposition;
2. *Grainstone:* grain-supported fabric, no mud, grains <2 mm in size;
3. *Packstone:* grain-supported fabric, with intergranular mud, grains <2 mm in size;
4. *Wackestone:* mud-supported fabric, with >10% grains, grains <2 mm in size;
5. *Mudstone:* mud-supported fabric, with <10% grains;
6. *Floatstone:* matrix-supported fabric, grains >2 mm in size;
7. *Rudstone:* grain-supported fabric, grains >2 mm in size.

Siliciclastic Sediment. For siliciclastic sediment, the principal name describes the texture and is assigned according to the following guidelines:

1. The Udden-Wentworth grain-size scale (Wentworth, 1922; Table 2) defines grain-size ranges and names of the textural groups (*gravel, sand, silt,* and *clay*) and subgroups (*fine sand, coarse silt,* etc.) that are used as the principal names of siliciclastic sediment. Note that the term *clay* is used only as a grain-size designation and neither denotes nor implies mineralogical composition.
2. Principal names are listed in order of increasing abundance when two or more textural groups or subgroups are present in a siliciclastic sediment (Shepard, 1954).
3. The suffix *-stone* is affixed to the principal names *sand, silt,* and *clay* when the sediment is lithified.
4. *Conglomerate* and *breccia* are used as principal names of gravels with well-rounded and angular clasts, respectively. The degree of lithification is designated by a modifier before the principal name.

Volcaniclastic Sediment. Volcaniclastic sediment is subdivided into two groups: *pyroclastic* and *epiclastic,* with the principal name in each group describing the texture. The names and ranges of three textural groups for pyroclastics (from Fisher and Schmincke, 1984) are as follows:

1. *Volcanic breccia:* pyroclasts >64 mm in diameter;
2. *Lapilli:* pyroclasts between 2 and 64 mm in diameter; when lithified, described as *lapillistone*;
3. *Ash:* pyroclasts <2 mm in diameter; when lithified, described as *tuff.*

Epiclastic sediments, like siliciclastic sediments, are classified by grain texture according to the Udden-Wentworth grain-size scale (Wentworth, 1922). The principal name describes the sediment texture and is preceded by the major modifier *volcanic* (e.g., volcanic conglomerate, volcanic sand, volcanic silt). To avoid confusion with coarse-grained pyroclastic rocks, the term *ig-lithic breccia* is used for sediment that contains large angular clasts of epiclastic origin. Other rules apply as listed previously for siliciclastic sediments. We also subdivided the fine-grained pyroclastic sediments of the ODP scheme into two size classes: material 1/16 to 2 mm in grain size (equivalent to sand in siliciclastic sediments) is described as *coarse ash* and material less than 1/16 mm (silt and clay size) is termed *fine ash. Coarse tuff* and *fine tuff* are the terms used for lithified equivalents of these size ranges.

Mixed Sediment. For mixed sediment, the principal name describes the degree of consolidation, using the terms *mixed sediments* or *mixed sedimentary rocks.*

Table 2. Udden-Wentworth grain-size scale for siliciclastic sediments (Wentworth, 1922).

Millimeters	μm	Phi (Ø)	Wentworth size class	
		-20		
4096		-12	Boulder (-8 to -12 Ø)	
1024		-10		
256		-8	Cobble (-6 to -8 Ø)	Gravel
64		-6		
16		-4	Pebble (-2 to -6 Ø)	
4		-2		
3.36		-1.75		
2.83		-1.50	Granule	
2.38		-1.25		
2.00		-1.00		
1.68		-0.75		
1.41		-0.50	Very coarse sand	
1.19		-0.25		
1.00		0.00		
0.84		0.25		
0.71		0.50	Coarse sand	
0.59		0.75		
1/2 — 0.50	500	1.00		
0.42	420	1.25		
0.35	350	1.50	Medium sand	Sand
0.30	300	1.75		
1/4 — 0.25	250	2.00		
0.210	210	2.25		
0.177	177	2.50	Fine sand	
0.149	149	2.75		
1/8 — 0.125	125	3.00		
0.105	105	3.25		
0.088	88	3.50	Very fine sand	
0.074	74	3.75		
1/16 — 0.0625	63	4.00		
0.0530	53	4.25		
0.0440	44	4.50	Coarse silt	
0.0370	37	4.75		
1/32 — 0.0310	31	5		Mud
1/64 0.0156	15.6	6	Medium silt	
1/128 0.0078	7.8	7	Fine silt	
1/256 — 0.0039	3.9	8	Very fine silt	
0.0020	2.0	9		
0.00098	0.98	10		
0.00049	0.49	11	Clay	
0.00024	0.24	12		
0.00012	0.12	13		
0.00006	0.06	14		

Major and Minor Modifiers

The principal name of a granular-sediment class is preceded by major modifiers and followed by minor modifiers (preceded by *with*) that describe the lithology of the granular sediment in greater detail (Table 1). Major and minor modifiers are used most commonly to describe the composition and texture of grain types present in major (>25%) and minor (10%–25%) proportions. In addition, major modifiers can be used to describe the degree of lithification, grain fabric, grain shape, and sediment color. The nomenclature for major and minor modifiers is outlined as follows. The composition of pelagic grains can be described with the major and minor modifiers *diatom(-aceous)*, *radiolarian, spicule(-ar)*, *siliceous, nannofossil, foraminifer(-al)*, and *calcareous.* The terms *siliceous* and *calcareous* are used generally to describe sediments composed of siliceous or calcareous pelagic grains of uncertain origins.

The composition of neritic grains can be described with the following major and minor modifiers:

1. *Ooid* (or *oolitic*): spherical or elliptical nonskeletal particles smaller than 2 mm in diameter, having a central nucleus surrounded by a rim with concentric or radial fabric;
2. *Bioclast(-ic)*: fragment of skeletal remains (specific names such as *molluscan* or *algal* can also be used);
3. *Pellet(-al)*: fecal particles from deposit-feeding organisms;
4. *Intraclast:* redeposited carbonate-rock fragment or rip-up clast;
5. *Pisolite:* spherical or ellipsoidal nonskeletal particle, commonly >2 mm in diameter, with or without a central nucleus, but displaying multiple concentric layers of carbonate;
6. *Peloid(-al)*: micritized carbonate particle of unknown origin;
7. *Calcareous, dolomitic, aragonitic, sideritic:* modifiers used to describe the composition of neritic grains.

The texture of siliciclastic grains is described by the following major and minor modifiers: *gravel(-ly)*, *sand(-y)*, *silt(-y)*, and *clay(-ey)*. The composition of siliciclastic grains can be described by the following:

1. Mineralogy: using modifiers such as *quartz, zeolitic, lithic* (for rock fragments), or *calcareous* (for detrital clasts of calcium carbonate);
2. Provenance: source of rock fragments (particularly in gravels, conglomerates, and breccias) can be described by modifiers such as *volcanic, sed-lithic* (contains clasts or grains of sedimentary rock), *basaltic,* and so forth.

Volcaniclastic grain composition is described by the following major and minor modifiers: *lithic* (rock fragments), *vitric* (glass and pumice), *volcanic sed-lithic* (contains clasts or grains of volcaniclastic rock), and *crystal* (mineral crystals and cleavage fragments), or by modifiers describing the composition of the lithic grains and crystals (e.g., *feldspar* or *basaltic*).

Sediment fabric can be described by the major modifiers *grain-supported, matrix-supported,* and *imbricated.* Generally, fabric descriptors are applied only to gravels, conglomerates, and breccias.

The degree of consolidation is described using the following major modifiers: *unlithified* designates soft sediment that is readily deformable under the pressure of a finger, *partially lithified* designates firm sediment that is incompletely lithified, and *lithified* designates hard, cemented sediment that must be cut with a saw.

Grain shapes are described by the major modifiers *rounded, subrounded, subangular,* and *angular.* Sediment color is determined with the Munsell Soil Color Charts (1975), a standard color-comparator, and can be employed as a major modifier.

Mixed sediments are described using major and minor modifiers indicating composition and texture.

X-ray Diffraction Analysis

A Philips ADP 3520 X-ray diffractometer was used for the X-ray diffraction (XRD) analysis of bulk samples. CuKΣ radiation with a Ni filter was used with a tube voltage of 40 kV and a tube current of 35 mA. Bulk samples were ground using the Spex 8000 Mixer Mill or with an agate mortar and pestle, pressed into a sample holder, and scanned from 2° to 70° 2θ, with a step size of 0.02° and a count time of 1 s per step.

STRUCTURAL GEOLOGY

Specialist structural studies have yet to become standard procedure on ODP legs. Exceptions include, for example, Leg 131 (Nankai Trough), during which specific objectives that could potentially be addressed by structural studies had been identified from the outset. Leg 135 was one of the first occasions on which an attempt was made to undertake an integrated approach to the study of tectonic features in ODP boreholes by means of the combination of separate and specially made visual core records with structural or orientation data acquired principally from downhole measurements and paleomagnetic studies.

This section deals with the structural core descriptions made aboard ship by the structural geologist. The intention of these records is to identify and describe in a way as systematic and quantitative as possible all the structural information (including bedding) present in the core and, in particular, to record its orientation. Apart from the whole-round samples taken immediately after core recovery for interstitial-water sampling, all material, from both working and archive halves, was examined.

Several problems are inherent in any study of this nature. From the point of view of the identification of tectonic features, commonly only part of the sampled interval in any one core is actually recovered. This leads to a sampling bias that for structural purposes is particularly acute: material from fault zones is that most commonly missing when recovery is less than 100%. When faulted rock from such zones is actually recovered it is typically highly disturbed relative to its original position. In addition, there is the difficulty of distinguishing between drilling-induced disturbance and real tectonic features. This is something that can be overcome with experience; however, a remaining problem is that many tectonic features appear to be obliterated by the drilling and core recovery processes. In general, planar structures that traverse a core and are associated with preserved fault rock may be regarded as original predrilling (i.e., tectonic) features rather than drilling induced. Cemented and/or mineral-lined fractures must likewise be real geological phenomena. Gently plunging striations or polishing marks may be drilling induced, but these can usually be distinguished readily from preexisting slickensides. Features were considered to be drilling induced if their origin was in doubt.

Recording the orientations of the observed structures is also difficult. Features must initially be oriented relative to local reference co-ordinates (i.e., the core liner reference frame) and subsequently corrected to true north and true vertical. Potentially, this can be done with the multishot orientation tool (with the APC system only), paleomagnetic data, and/or the borehole televiewer (BHTV) and formation microscanner (FMS). With the APC in soft sediments, recovery is generally relatively complete and drilling should not rotate the core within its liner to any significant degree.

Sections from individual core barrels should therefore be internally consistent in relation to their local reference frames and true north. Any correction needed can be made if the multishot tool is used (see the following). For XCB and rotary coring, however, drilling disturbance is much more common and the multishot orientation tool cannot be run. In basement, rotary drilling causes the rotation of individual pieces of core, such that relative rotation in any individual sections or core barrels occurs, and correction back to true north may be different for each piece of sample. Furthermore, the reference line for each reconstructed piece in basement rocks is drawn arbitrarily, following visual inspection by the igneous petrologists, so this temporary reference orientation may potentially be consistent over only a few tens of centimeters.

Description and Measurement of Structures

The description and measurement of structures are based on both halves of the split core, as information from the two is usually complementary. Initial data are recorded on a special working-core description form; these are later entered into a separate spreadsheet for core orientation correction. The working-core description form has several broad columns to allow the working space and flexibility necessary while handling the cores; the spreadsheet, in contrast, has rigorously defined columns so as to prompt consistent and quantitative recording and later transformation of the data. Both were modified during the course of the leg.

Bedding in Sediments

Unlithified and partly lithified sediments cannot easily be removed from the core liners, so the determination and measurement of the orientation of bedding planes and so forth cannot be made directly without disturbance of the core. Instead, the system of apparent dips that was used is based principally upon examination of the working half of the core. The apparent dip in the plane of the cut surface was measured using a protractor or a clinometer (Fig. 7) and its sense recorded (i.e., whether the bedding plane dips to the left or to the right when looking up the axis of the core). A vertical incision was then made, using a metal scoop, parallel to the axis of the core, and a quarter-round sample (including the bedding plane) temporarily removed to expose a new face perpendicular to the original split-core surface. A second apparent dip was then measured on this new face, and the sense (i.e., whether the apparent bedding surface dips toward the "top" or "bottom" of the core) recorded. The potential errors inherent in this technique (assuming that the apparent dips can be measured to the nearest degree) are high for gently dipping sediments, but are much lower for moderately dipping strata (Fig. 8).

A temporary dip and strike, measured relative to the cut surface of the core may be made using stereographic projection to fit a

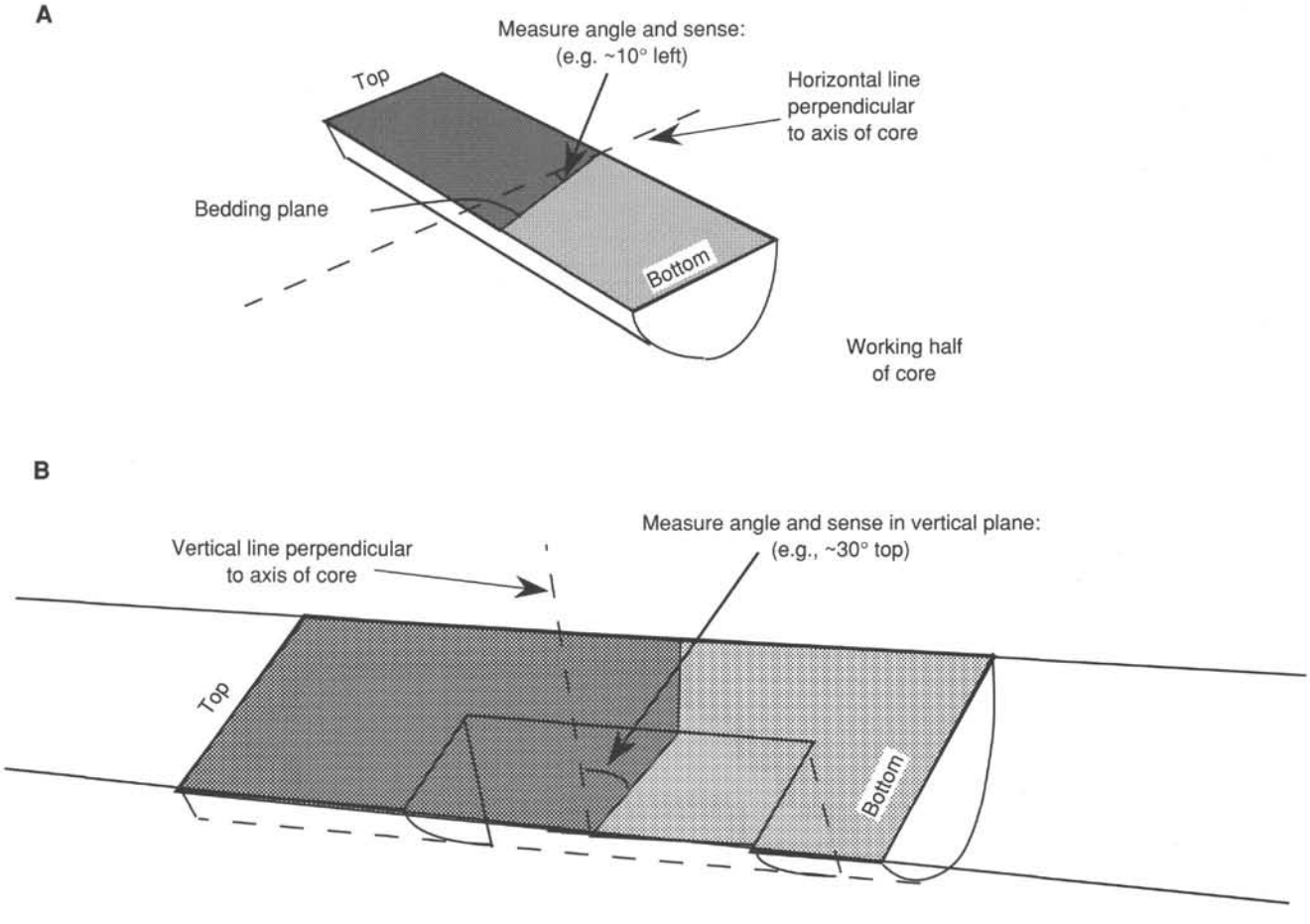

Figure 7. Method of measurement of the orientation of bedding in poorly lithified sediments. **A.** The apparent dip in the plane of the cut face of the working half of the core is measured, and the sense of dip indicated (i.e., whether down to the left or to the right when the top of the core is pointing up). **B.** A quarter-round sample of core is removed with a metal scoop to expose a new (vertical) face perpendicular to the main cut face. The apparent dip of this face is also measured, and the dip indicated (whether toward the top or bottom).

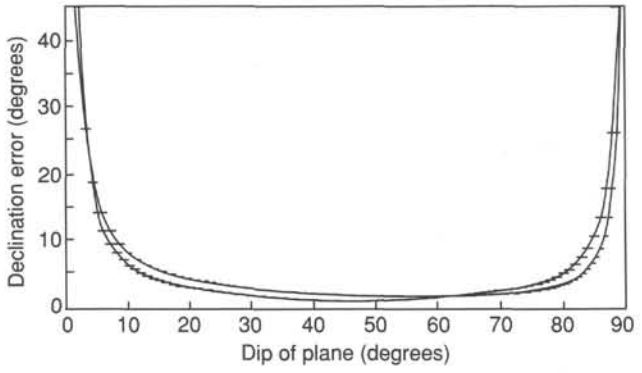

Figure 8. An estimation of the declination error inherent in the measurement of bedding orientation derived from two apparent dips (as in Fig. 7). The curves are calculated assuming that the apparent dips can be measured to the nearest degree; the symmetrical curve is for a plane dipping toward one of the apparent dip axes and the asymmetrical curve for a plane dipping at 45° to the two apparent dip axes. Note that the errors are very high for near-horizontal strata, but decrease abruptly for moderately dipping bedding: for a dip of 15°, for example, the declination error is approximately ±5°.

great circle to the two apparent dip lines. Alternatively assignment may be made later, at the same time as correction is made to geographic coordinates, when paleomagnetic and/or downhole geophysical information becomes available.

Veins, Fractures, and Other Features

The measurement of planar features traversing the core at oblique angles can be made in several ways. The convention adopted during Leg 135 and illustrated in Figure 9 is modified slightly from that used during Legs 131 and 134. The plane normal to the axis of the borehole is referred to as the apparent "horizontal" plane. On this plane a 360° net is used with a pseudonorth (0°) at the bottom line of the working half of the core, the same convention as that used by the paleomagnetists. The face of the split core therefore lies in a plane striking 90°-270° and dipping vertically. An apparent dip can be measured on this surface, and its sense (whether toward 90° or 270°) indicated. If the feature to be measured is conveniently oriented relative to the cut, the azimuth and dip of the strike line can be measured directly; otherwise, the measurement of one further apparent dip on whichever surfaces are accessible is required to obtain a (relative) orientation, as described previously. Dips recorded at this stage all assume that the core was vertical; if data from, for example, the general purpose inclination tools, suggest otherwise, a correction can be made on the spreadsheet template.

Linear structures such as slickensides can be measured in a similar fashion: either directly, by their azimuth and amount of plunge, or indirectly, by means of their pitch on a previously measured plane. The sense of movement of some linear structures can be ascertained, allowing the distinction between components of normal vs. reverse and/or sinistral vs. dextral motion. The magnitude of displacement may be visible, and can be measured directly, if the fault surface is visible, or calculated from the apparent offset on the cut surface of the core.

Methods of Orienting Core

Following the recording of orientation data, it is necessary to convert as many of these local orientations as possible to geographical co-ordinates. The three ways in which this may be achieved involve the multishot orientation tool, paleomagnetic data, and downhole logging.

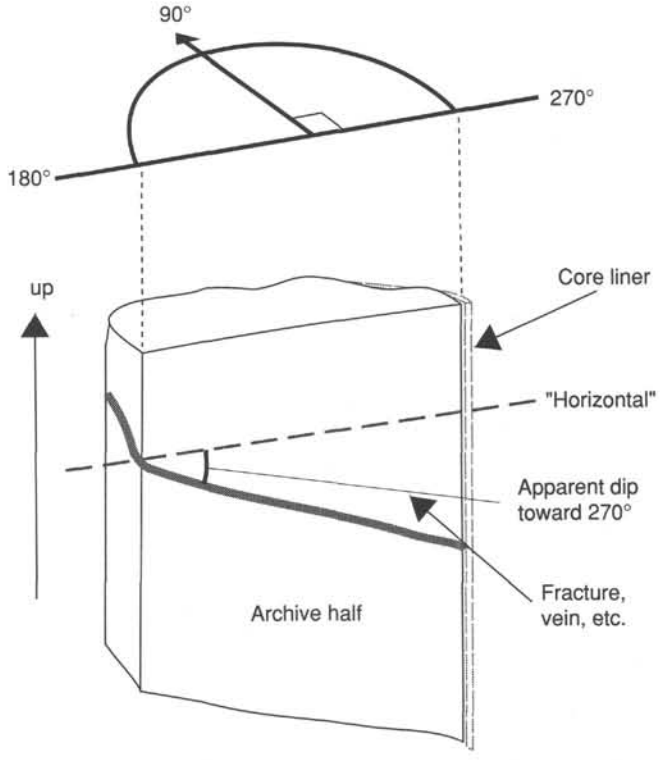

Figure 9. The convention used for the measurement of azimuths and dips on structural features in lithified and/or basement core. The temporary qualifiers left, right, bottom, and top in Figure 7 can be referred to the (still nongeographic) coordinates 270°, 90°, 0°, and 180°, respectively.

Multishot Orientation Tool

The multishot orientation tool consists of a compass that is lowered downhole and photographed next to the plastic core liner, such that the orientation of the reference marks on the liner relative to magnetic north are visible. It has been unreliable in the past (e.g., Leg 131) and was found to be so during Leg 135 (see "Paleomagnetics" and "Structural Geology" sections in the chapters for Sites 834, 835, and 838, this volume). Its use for structural studies is severely handicapped because it can be employed only with the APC system, and therefore only in the uppermost, barely lithified, sedimentary sections of each hole.

Paleomagnetic Data

Paleomagnetic analysis provides a way of orienting individual sections of core on a small scale and is especially useful for basement cores obtained by XCB or rotary coring, which typically recovers contiguous pieces of core ranging from only a few centimeters up to about 1 m in length. Data from the routine analysis of the archive halves of the core made by the shipboard paleomagnetists using a cryogenic magnetometer with demagnetization up to 15 mT can be used to orient sections of core. To obtain data from samples shorter than the averaging length of the magnetometer (typically 10 cm), individual pieces of sufficient length from the working half of the core can be run through the instrument without demagnetization, if the drilling-induced component of magnetization is not too strong. The declination and inclination of the natural remanent magnetization determined by both these methods can be used to orient larger pieces of core, assuming that no significant tectonic rotation of the sample occurred. These techniques cannot, however, account for secular variations in the Earth's magnetic field. For samples that acquired their magnetic characteristics rapidly (i.e., for igneous rocks),

variation in the order of ±15° in declination and inclination is to be expected. This probably accounts for some of the scatter observed in plots of, for example, joint trends in the igneous portions of Hole 834B (see "Structural Geology," "Site 834" chapter).

Downhole Logging

On Leg 135 the FMS and analog BHTV logging tools were used. Both of these tools make an "image" of the borehole wall: the FMS measures variations in resistivity by means of pads pressed against the wall, and the BHTV is an ultrasonic tool that maps acoustic reflections from the borehole (see "Downhole Measurements" section, this chapter). Both carry fluxgate magnetometers that allow orientation of the processed images. The BHTV is particularly sensitive to the borehole geometry, readily picking out fractures and basement features, whereas the FMS is better at distinguishing sedimentary bedding. Both can be used in their own right as structural tools, and this is discussed elsewhere; however, they are also of use in the orientation of sections of core. The difference between the diameter of the borehole and that of the core is such that the identification of individual features on both cannot be made directly and may be difficult; they can be used most successfully for orientation purposes when, for example, regularly inclined bedding or a single, regular joint pattern can be recognized on downhole images and correlated with the core-derived data.

Downhole logging is most powerful in this context when used in conjunction with paleomagnetic data, as it potentially allows the identification of possible tectonic rotations of the magnetization vector, which otherwise would have to be assumed to be zero.

BIOSTRATIGRAPHY

Calcareous nannofossils and planktonic foraminifers were analyzed during Leg 135 for biostratigraphic purposes. Age assignments are based mainly on core-catcher samples, which were taken from the bottom of each core that contained sediment. Additional samples from within the cores were examined when a critical shipboard age determination was necessary. Larger benthic foraminifers were present at Site 841 and were analyzed for biostratigraphic and paleoenvironmental information.

The general correlation between the biostratigraphic zones and the magnetic polarity reversal record is based on the time scale of Berggren et al. (1985b) with minor differences (Fig. 10). These differences are discussed in the individual sections for a particular fossil group. A paleontology summary chart for each site shows the correlation of lithostratigraphy and biostratigraphy to magnetostratigraphy (Fig. 11).

Calcareous Nannofossils

Zonation

The calcareous nannofossil zonal schemes used during Leg 135 are those of Martini (1971), Bukry (1973, 1975), and Okada and Bukry (1980) with minor modifications.

Sample Preparation

Smear slides were prepared for each sample using Piccolyte as a mounting medium. The calcareous nannofossils were examined on the slides using light microscopy techniques (plane-polarized light, phase contrast, and cross-polarized light) at approximately 980× magnification.

Abundance and Preservation

The abundance of nannofossils was estimated by traversing up to 100 fields of view across a slide and assigning the following categories:

VR = very rare (1 specimen per 100 fields of view);
R = rare (2–5 specimens per 100 fields of view);
F = few (2–10 specimens per 10 fields of view);
C = common (2–20 specimens per field of view);
A = abundant (20–100 specimens per field of view); and
VA = very abundant (>100 specimens per field of view).

The state of preservation was estimated as follows:

G = good (little or no evidence of dissolution or secondary overgrowth of placoliths and discoasters);
M = moderate (dissolution and/or secondary overgrowth partially alter primary morphological characteristics, but nearly all specimens can be identified at the species level); and
P = poor (severe dissolution, fragmentation and/or secondary overgrowth with primary features largely destroyed; many specimens cannot be identified at the species and/or generic level).

Planktonic Foraminifers

Zonation

The planktonic foraminiferal biostratigraphic scheme followed in this volume is based on that of Blow (1969), as modified by Kennett and Srinivasan (1983) for the Miocene and Pliocene, and by Chaproniere (in press) for the Pleistocene. The correlation of the planktonic foraminiferal zones to the magnetic polarity scale follows mainly the scheme of Berggren et al. (1985b). However, the first occurrence of *Globorotalia truncatulinoides* at Site 834 is in the Gauss. This is earlier than that reported by Berggren et al. (1985b) and agrees with the findings of Dowsett (1989) at Site 590 in the southwest Pacific. We have also constrained the last occurrence of *Globigerinoides fistulosus* to N22 at the level of the last occurrence of *Discoaster brouweri*. With the exception of *Globorotalia truncatulinoides*, as explained previously, the ages of various key taxa used for age-depth plots follow the usage of Berggren et al. (1985b) and Chaproniere (in press).

Sample Preparation

All samples were disaggregated using a solution containing 30% hydrogen peroxide, with Calgon added to clay-rich and more indurated samples. After soaking, the samples were washed over a 63-μm sieve. Washed residues were washed in alcohol and dried over a hot plate. The washed residue was then strewn over a gridded tray so that abundance estimates could be made.

Abundance and Preservation

For estimates of species abundance the following scale was used:

R = rare (1–5 tests on tray);
F = few (6–10 tests on tray);
C = common (11–25 tests on tray); and
A = abundant (>25 tests on tray).

The preservational state is described as follows:

G = good (little or no fragmentation);
M = moderate (some signs of fragmentation or alteration); and
P = poor (severe fragmentation or alteration).

SEDIMENT ACCUMULATION RATES

Sediment accumulation rates were estimated from age-vs.-depth data for each site. Absolute ages follow the Cenozoic time scale as outlined in the preceding "Biostratigraphy" section. Paleomagnetic data from each site were calibrated to the calcareous

microfossil biostratigraphic events. A table of the events used as well as the age-depth plots are given in each of the site chapters.

Biostratigraphic data were used as a first estimate of the age of the sediments at each site from the time scale used in this volume. This permitted the correlation of the paleomagnetic data to the published paleomagnetic time scale, which yielded age determinations that were used to adjust the age estimates for the stratigraphic section.

Periods of continuous sedimentation on the age-depth curves are indicated by solid lines, and hiatuses are denoted by dashed lines. Average rates of sedimentation during each epoch are given within each figure.

PALEOMAGNETICS

Two types of magnetic measurements, volume magnetic susceptibility (MS) and remanent magnetization, were routinely made during Leg 135. MS was used as a tool for highlighting sediment and igneous core variations by magnetic character. Such measurements typically show correlation with gross lithologic variations, such as ash layers or turbidites. However, it was also felt that MS values might also show subtle environmental and geologic changes within the sediments.

Remanent magnetization measurements were made to determine magnetic polarities so that core material might be dated by reference to the geomagnetic polarity reversal time scale. For this, primarily the time scale of Berggren et al. (1985a) was used. However, dates for the Cobb Mountain Event and Réunion Subchron were taken from Clement and Robinson (1987) and Harland et al. (1982), respectively. As relatively high sedimentation rates were expected, it was also hoped that the cored sediments might contain expanded records of geomagnetic polarity transitions suitable for detailed study as well as cyclical magnetic property variations potentially related to Milankovitch climate cycles. Finally, remanent magnetization measurements were made to examine the tectonic history of the opening of the Lau Basin by differences in the magnetic declination of samples taken from the Lau Basin and Tonga Ridge. For this study, core material was azimuthally oriented in two ways: (1) the multishot orientation tool for APC cores and (2) comparison of dipping beds and fractures in the cores with downhole FMS and BHTV logs (see "Structural Geology" section, this chapter).

Magnetic Susceptibility

Volume MS measurements were obtained from whole, unsplit 1.5-m core sections using a Bartington Instruments model MS-1 susceptibility meter with an 80-mm sensing loop. Readings were typically taken at spacings of 3 to 5 cm. Almost all APC cores were measured; however, because core susceptibility varies with its volume, XCB and rotary cores were measured only if the core cross sections were relatively consistent.

Volume MS, k, is a dimensionless scalar quantity relating the applied magnetic field vector, H, and the magnetization, M, that it induces in a material:

$$M = kH.$$

In sediments and rocks, MS is a measure of the amount of magnetizable material (usually magnetite), but it is also sensitive to magnetic grain size and shape. Because the shipboard MS data-gathering and -processing computer programs are set up for cgs units, these are used in the site chapters. A conversion to standard SI units is easily made by the multiplication of these values by a constant,

$$k_{cgs} = 4\pi k_{si}.$$

The Bartington MS meter has a sensitivity of 1×10^{-7} cgs, but on Leg 135 the weakest sediments measured had MS values 1–2 orders of magnitude higher.

Remanent Magnetization

Remanent magnetization measurements were made with two instruments, a 2-G Enterprises model 760R pass-through cryogenic magnetometer and a Molspin Minispin spinner magnetometer. The former was used to measure the archive halves of split APC cores and selected XCB and RCB cores using a spacing of 5 cm. The pass-through magnetometer's sensitivity to weakly magnetized samples is limited by the moment of the "boat" that carries the core section through the sensing region, about 2.5×10^{-6} emu (2.5×10^{-9} Am^2). For strongly magnetic samples, the magnetometer's practical upper limit is a magnetization somewhat greater than 1 A/m. Core material from Leg 135 was typically strongly magnetic, particularly if the cored interval contained igneous rocks or their derivatives. Even the sediments had generally strong magnetizations, some approaching 1 A/m.

Because the sensing region of the pass-through magnetometer is about 20 cm in length, it smoothes variations in core magnetization. To obtain independent magnetization measurements at spacings less than about 20 cm, the magnetometer output must be deconvolved. This could not be done during Leg 135 as no deconvolution routine was available aboard *JOIDES Resolution*. At worst, the large sensing region makes it inappropriate to measure cores that are broken into small pieces or that are pervasively disturbed. XCB sediment cores were commonly broken into biscuits only a few centimeters in thickness that had been rotated about a vertical axis. Consequently, XCB cores were not typically measured with the pass-through magnetometer. Likewise, RCB cores suffered similar deformation; however, long pieces were obtained sporadically in these cores and measured.

A problem with most of the core sections measured on Leg 135 was a pervasive overprint directed upward along the core axis. This phenomenon has been noted on other ODP cruises (e.g., Legs 107, 115, and 116) and attributed to the magnetization of core material by exposure to large magnetic fields emanating from the core barrel and drill string. The pass-through cryogenic magnetometer has a built-in alternating field (AF) demagnetizing coil, the purpose of which is to remove such spurious magnetization components. Although its use removed much of the drill-string overprint, the ODP 15-mT limit on demagnetizing archive halves made it impossible to remove the entire overprint.

Discrete samples were obtained from soft sediments by cutting a 7-cm^3 sample and placing it in a plastic cube. Indurated sediments and igneous rocks were sampled by drilling a 1-in.-diameter minicore or cutting a 1-in. cube with the rock saw. Samples were taken perpendicular to the split face of the core and oriented with a fiducial mark pointing upcore. Discrete samples were measured with the Molspin spinner magnetometer and magnetically cleaned using a Schonstedt GSD-1 AF demagnetizing unit. Isothermal remanent magnetization (IRM) curves were made for a few discrete samples using a pulse magnetizer capable of achieving fields up to 0.9 T. Such curves give an indication of the type of magnetic grains contained in a sample.

Core Orientation

Many APC cores were oriented for paleomagnetic work by using the Eastman-Whipstock multishot orientation tool. This device is a small camera that takes photographs at predetermined intervals of an orientation unit that consists of a compass and pendulum inclinometer. It is installed in a pressure housing on the sinker bar assembly of the APC core barrel. Before firing, the APC is held still for several minutes to allow a few clear orientation

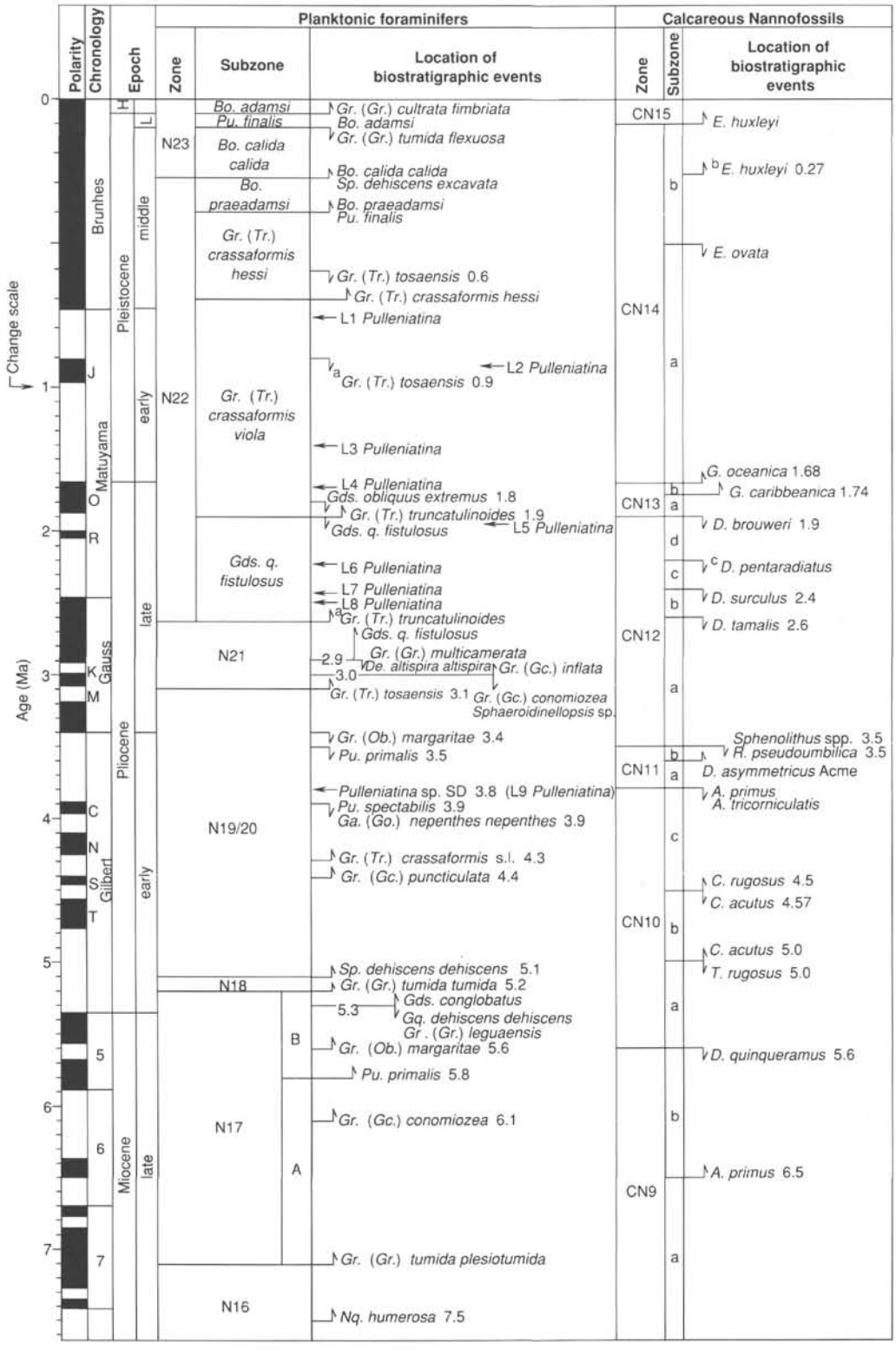

Figure 10. Biostratigraphic standard for Leg 135.

[a]Event position based on results of this cruise or on Dowsett (1989).

[b]Age in Ma from Berggren et al. (1985b, p. 247); approximates the base of CN15 of Okada and Bukry (1980).

[c]Berggren et al. (1985b, p. 185) list the LAD of both *D. pentaradius* and *D. surculus* as 2.4 Ma. Bukry (1975) suggests that *D. surculus* disappears before *D. pentaradiatus*. We, therefore, place the LAD of *D. pentaradiatus* an arbitrary distance above the LAD of *S. surculus*.

[d]Planktonic foraminifer zones from Berggren and Miller (1988); larger foraminifer zones from Adams (1970) and Chaproniere (1981, 1983).

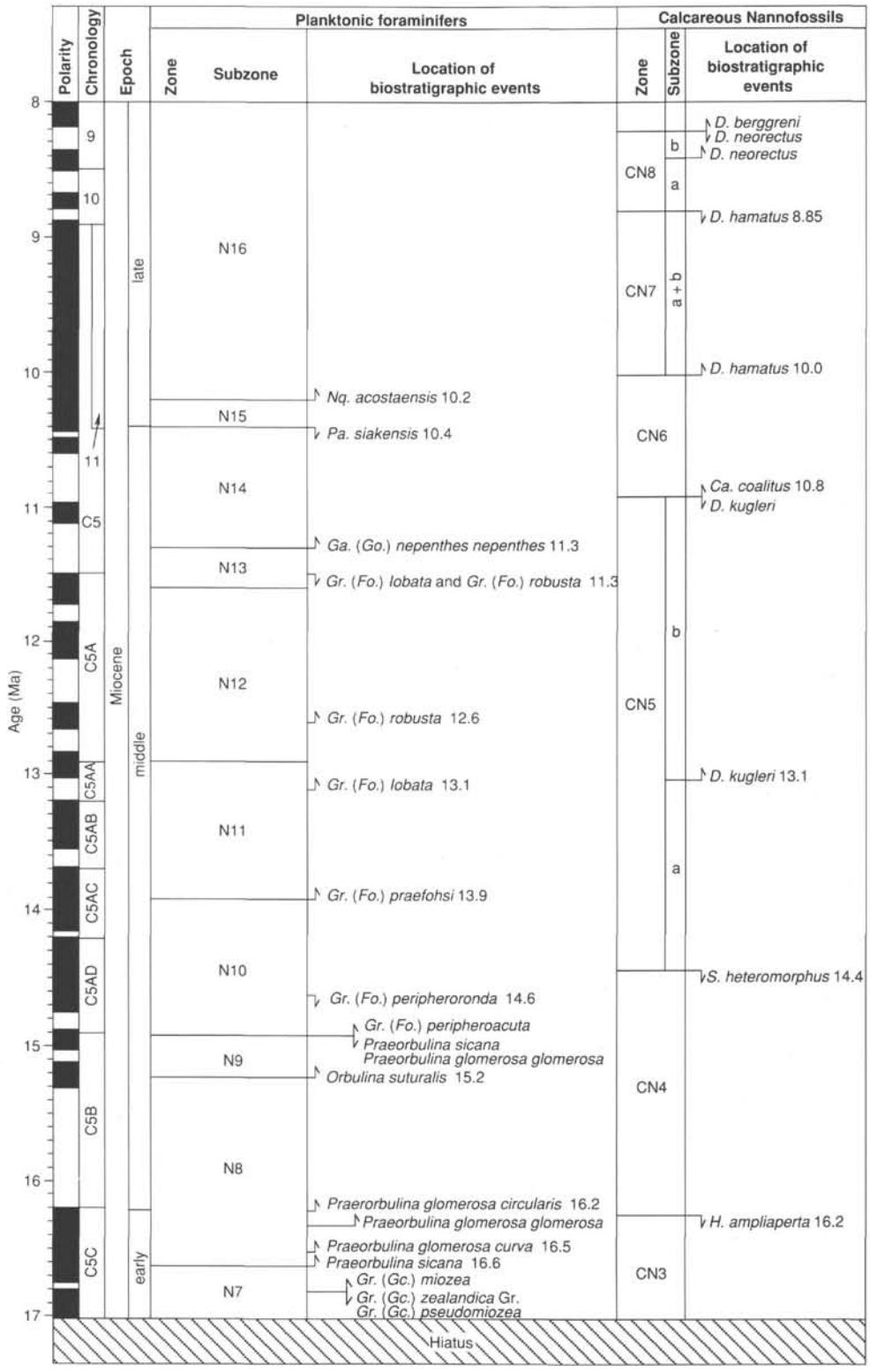

Figure 10 (continued).

photographs to be made. The multishot tool yields the orientation of the APC relative to magnetic north. The APC and core liner are aligned so that the camera records the angle between magnetic north and the double lines on the core liner (the working-half side). During Leg 135 it was discovered that one of the two orientation units was misaligned with the fiducial mark. This error was measured at 13° and affected the unit called "Compass B" in the text. In all tables of orientation data, the raw orientation data are provided. The 13° error must be added to the listed declination of Compass B to correct that datum.

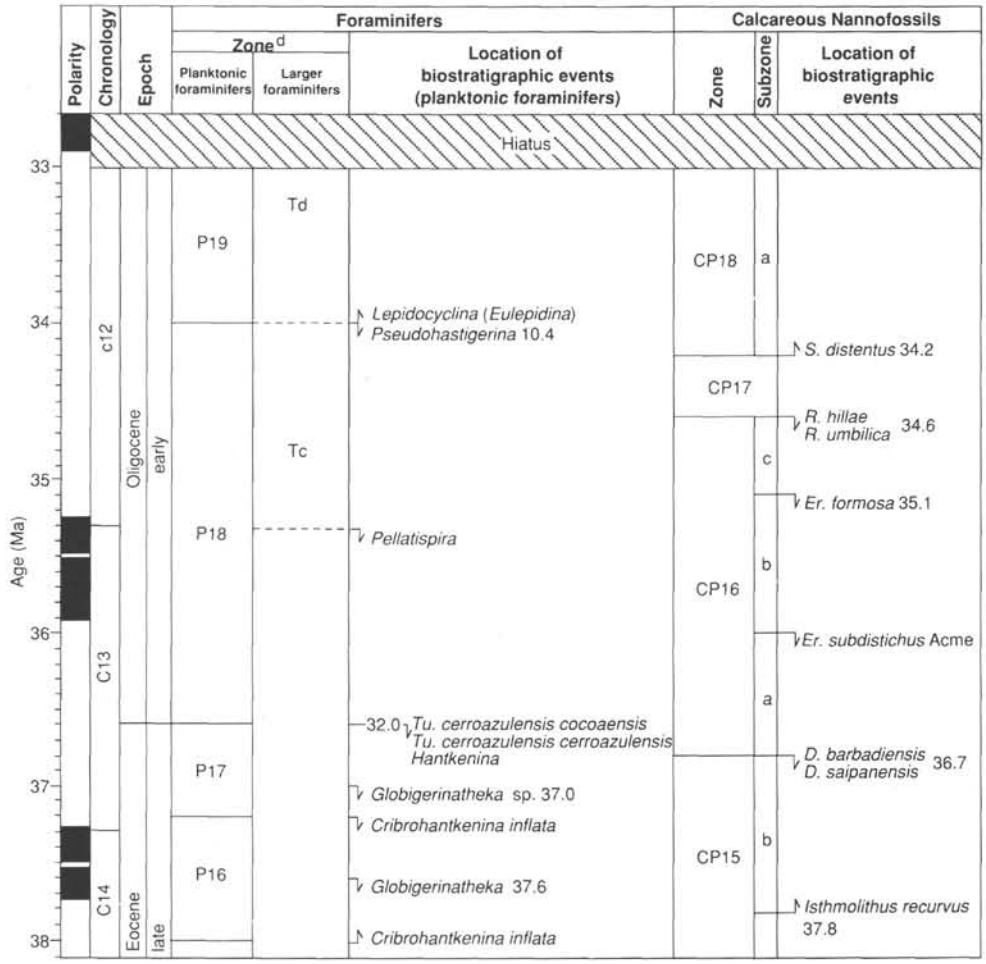

Figure 10 (continued).

INORGANIC GEOCHEMISTRY

The inorganic geochemistry program for Leg 135 included (1) analyses of the interstitial waters for pH, alkalinity, salinity, sulfate, chlorinity, calcium, magnesium, potassium, strontium, silica, ammonia, and manganese and (2) measurement of the dissolved hydrocarbon gases (C_1, C_2, and C_3).

The method of obtaining interstitial waters from the sediment, using a stainless steel press, was described in detail by Manheim and Sayles (1974). For the interstitial water analyses, whole-round sediment core samples 10 cm in length were collected immediately after the core arrived on deck. The sediment was extruded from the core liner, the outer layer of the sediment was removed by scraping with a spatula, and the sample was placed in a Carver laboratory press for removal of the interstitial water. The press was operated to a pressure of about 30,000 psi (2.11 kg/m^2). The sediment sample remained under pressure until water could no longer be squeezed from it. Interstitial water was collected in 50-cm^3 syringes and filtered through a 0.45-mm Millipore filter. International Association for the Physical Sciences of the Ocean (IAPSO) standard seawater P99 was the primary standard for the water analysis aboard ship.

Individual inorganic species were analyzed according to the procedures outlined by Gieskes and Peretsman (1986). Results are expressed in millimoles or micromoles per liter of solution. Sodium concentrations were determined by charge balance; the difference between calculated salinity using Na data and measured salinity never exceeded 3%.

Alkalinity and pH were determined using a Metrohm autotitrator with a Brinkmann combination pH electrode. Alkalinity reproducibility is better than 5%; data are given in millimoles of acid equivalent per liter. Salinity was determined using a Goldberg optical hand refractometer measuring the total dissolved solids. Chlorinity was measured by silver nitrate titration of a 0.1-mL sample diluted in 5 mL of deionized water using potassium chromate as an indicator. Reproducibility of the IAPSO standard is better than ±1%. Sulfate was quantified using a Dionex 2120 ion chromatograph. Reproducibility on different dilutions of the IAPSO standard is better than ±2%.

Calcium was determined by complexometric titration of a 0.5-cm^3 sample with EGTA (ethylene-bis-(oxyethylenenitrilo)-tetra-acetic acid) using GHA (2-2′-ethane-diylidine-dinitrilo-diphenol) as an indicator. To enhance the determination of the end point, the calcium-GHA complex was extracted onto a layer of butanol (Gieskes, 1973). No correction was made for strontium, which is also included in the result. Magnesium was determined by EDTA (di-sodium ethylenediamine-tetra-acetate) titration for total alkaline earths (Gieskes, 1973). Subsequent subtraction of the calcium and strontium values yielded the magnesium concentration in the interstitial water sample. Ammonia and silica determinations were carried out using the colorimetric methods described by Gieskes and Peretsman (1986).

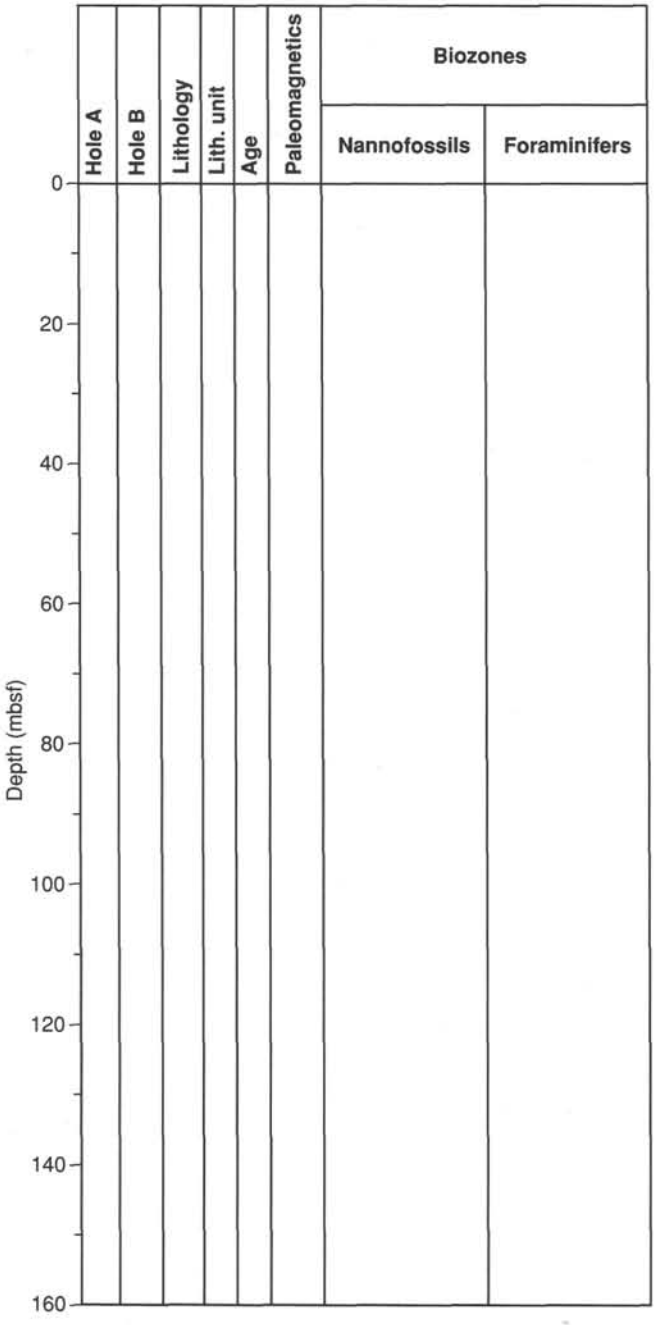

Figure 11. Paleontology summary chart.

Atomic absorption measurements were done with a Varian SpectrAA-20 spectrophotometer to determine K, Sr, and Mn. All measurements were done in absorption mode using an oxidizing air-acetylene flame. Potassium was determined on 1:500 sample dilutions with 1000-ppm cesium chloride as an ionization suppressor. Standards used range from 0.25 to 1.50 ppm with a correlation coefficient $r = 0.9996$. Reproducibility is about ±3%. Strontium was determined on 1:20 sample dilutions. Lanthanum trichloride (5000 ppm) was used as a buffer in the sample solution and in the standards. The standard calibration curve ranges from 1 to 5 ppm. The linear correlation coefficient obtained is $r = 0.9998$. Reproducibility is better than ±2%.

Manganese was determined on 1:5 dilutions of the samples. A 1000-ppm cesium chloride solution was used as an ionization suppressor in the sample solution and in the standards. The standard calibration curve ranges from 0.25 to 3 ppm with a correlation coefficient $r = 0.9995$. The detection limit of this method is about 20 mM in the sample and the reproducibility is better than 2% for Mn concentrations higher than 50 mM.

The sampling method for interstitial-water dissolved methane analysis was that used during the "Hydrotherm" expedition to the Atlantis II Deep (Blanc et al., 1986, 1990) and on Leg 110 (Moore, Mascle, et al., 1990). Sediment samples for this analysis were taken immediately upon arrival of the cores on deck. A small volume of sediment was placed in a borosilicate glass vial, and the vial was then filled to approximately two-thirds of its total volume with sodium azide-poisoned, hydrocarbon-free seawater. The sodium azide (NaN_3) inhibits any possible microbial activity after sampling. The vial was then capped and sealed with an aluminum ring. The sample was agitated on a high-speed shaker to partition gas into a helium-filled headspace similar to the method used by Bernard et al. (1976, 1978). The headspace methane was analyzed by gas chromatography on a Hewlett-Packard 5890A. Methane concentrations are expressed in micromoles per liter of the pore water, calculated from the sediment dry weight and original water content (see "Physical Properties" section, this chapter).

ORGANIC GEOCHEMISTRY

Shipboard organic geochemistry during Leg 135 was conducted to supply a real-time monitoring of volatile hydrocarbons for safety considerations and for an initial characterization of the content and type of gases and sedimentary organic matter. These analyses provide a basis for the preliminary site summaries and background for the more detailed shore-based studies.

Gas Analyses

As required by safety considerations, the concentrations of the hydrocarbons methane (C_1), ethane (C_2), and propane (C_3) were monitored in the sediment cores at intervals of approximately 9.5 m.

Gases were extracted from bulk sediments utilizing headspace-sampling techniques (Emeis and Kvenvolden, 1986). A no. 4 cork borer was used to take a 5-cm^3 plug of sediment as the core arrived on deck. The sample was placed immediately into a glass vial, sealed with a septum and metal crimp, and heated to 70°C and kept at this temperature for 45 min.

Gas-pocket samples were obtained by expanding gases from visible pockets into preevacuated and sealed glass tubes (vacutainers). For this purpose, one end of an injection needle was inserted through the rubber stopper of the vacutainer and the other end through the plastic liner into the gas pocket.

All headspace gas and vacutainer samples were expanded into a gas-tight syringe and injected into one of the following depending on gas concentration:

1. Hach-Carle AGC series 100 model 211 gas chromatograph equipped with a flame ionization detector and a 6-ft × 1/8-in. steel column packed with Poropak N:Q (80%/20%);
2. Hewlett-Packard 5890A Natural Gas Analyzer (NGA) gas chromatograph for flame ionization detector (FID) and thermal-conductivity detector (TCD) analyses. The gas chromatographic system employs a 6-in. × 1/8-in. steel column packed with Poropak T, a 3-ft × 1/8-in. stainless steel column with a 13× molecular sieve, a 6-ft × 1/8-in. steel column packed with 80/100 mesh Hayesep R (acid wash), and a DB1 (1-mm film thickness, J&W). Appropriate automatic valve switching, controlled by a Hewlett-Packard 3392 Integrator, which also recorded and integrated the count rates, provided a rapid determination of oxygen, nitrogen, carbon dioxide, and hydrocarbons from methane to hexanes. The separation

on the FID line was carried out isothermally at 40°C at a flow rate of 2.24 mL/min. Helium was used as the carrier gas.

The NGA chromatograph was used only when higher concentrations of gas were found. All gas concentrations are reported in parts per million (ppm).

Elemental Analyses

Sediments were analyzed on board for inorganic carbon and for total nitrogen, carbon, and sulfur. The total organic carbon (TOC) content of the sediments was then calculated by subtracting the inorganic carbon content from the total carbon content. The analyses were carried out on sediment residues from headspace gas analyses, and the sediments were freeze-dried before being analyzed. The value obtained from Rock-Eval analysis was also used for a sample with a higher TOC (>0.5%) value.

Total inorganic carbon was determined using a Coulometrics 5011 coulometer equipped with a System 140 carbonate carbon analyzer. Depending on carbonate content, 15 to 70 mg of ground and weighed sediment was reacted in a 2N HCl solution. The liberated CO_2 was titrated in a monoethanolamine solution with a color indicator, while the change in light transmittance was monitored with a photodetection cell.

Total nitrogen, carbon, and sulfur were determined using an NA 1500 Carlo Erba NCS analyzer. Bulk samples were combusted at 1000°C in an oxygen atmosphere with the addition of vanadium pentoxide, converting organic and inorganic carbon into CO_2 and sulfur to SO_2. These gases along with nitrogen were then separated by gas chromatography and measured by TCD analysis.

Rock-Eval Analyses

The bulk geochemical character of sedimentary organic matter was determined utilizing Rock-Eval-II pyrolysis techniques outlined by Espitalié et al. (1985a, 1985b, 1986). This technique permits a rapid identification of the type and maturity of the organic matter in ground rock samples of about 100 mg. The pyrolysis technique involves a microprocessor-controlled temperature program that causes the release of hydrocarbons and CO_2 in a stream of helium. The amount of hydrocarbons is determined by an FID, whereas for CO_2 the TCD method is employed. Four parameters characterizing the organic matter were determined:

1. S_1: the amount of free hydrocarbons in the sample (mg hydrocarbons per g of rock) recorded at pyrolysis temperatures below 300°C.
2. S_2: the amount of hydrocarbons generated through thermal cracking of the kerogen as the sediment is heated at 25°C/min from 300°C to 550°C during pyrolysis (cycle 1). S_2 is an indication of the quantity of hydrocarbons that could be produced in this rock, should burial and maturation continue.
3. S_3: the quantity of CO_2 (mg CO_2 per g of rock) produced from pyrolysis of the organic matter at temperatures between 300° and 390°C is detected by the TCD and recorded during cooling.
4. T_{max}: maturity of the organic material assessed by the temperature at which a maximum release of hydrocarbons from cracking of kerogen during pyrolysis occurs (top of the S_2 peak).

The Rock-Eval also provides information on the type of organic matter through the hydrogen index ($HI = [(100 \times S_2)/TOC]$), oxygen index ($OI = [(100 \times S_3)/TOC]$), and S_2/S_3 ratio.

Rock-Eval pyrolysis was only carried out on those sediment samples that were thought likely to be organic rich because it is considered unreliable for samples with less than 0.5% TOC.

IGNEOUS ROCKS

Core Curation and Shipboard Sampling

To preserve the important features and structures, core sections containing igneous rocks were examined before they were split. During core handling and splitting, core orientation was preserved by carefully marking the original base of individual pieces. Each piece was numbered sequentially from the top of each core section and labeled at the top surface. Pieces that could be fit together were assigned the same number and lettered consecutively (e.g., 1A, 1B, 1C), even if they occupied more than one section. Plastic spacers were placed between pieces with different numbers. The presence of a spacer, therefore, may represent a substantial interval of no recovery. If it was evident that an individual piece had not rotated about a horizontal axis during drilling, an arrow was added to the label pointing to the top of the section. As all pieces were free to turn about a vertical axis during drilling, azimuthal orientation of the core was not possible. After the vertical core orientation was noted, the pieces were split with a diamond saw into archive and working halves, with care taken to ensure the division of key features.

After the core was split, the working half was sampled for shipboard physical properties, paleomagnetic, X-ray fluorescence, X-ray diffraction, and thin section studies. Nondestructive physical properties measurements, such as magnetic susceptibility, were made on the archive half of the core. Where recovery permitted, samples were taken from each lithologic unit. The archive half was described using the visual core description form and was photographed before storage.

Visual Core Description Forms

Visual core description forms were used in the documentation of the igneous rock cores (see appendixes). The left-hand column is a graphic representation of the archive half. A horizontal line across the entire width of the column denotes a plastic spacer. Oriented pieces are indicated on the form by an upward-pointing arrow to the right of the piece. Shipboard samples and studies are indicated in the column headed "Shipboard Studies," using the following notation: D = X-ray diffraction analysis, F = X-ray fluorescence analysis, T = petrographic thin section, P = physical properties analysis, and X = paleomagnetic analysis.

To ensure consistent and complete description, the visual core description forms were entered into the computer database HARVI. The database is divided into separate data sets for fine- and coarse-grained rocks. Each record is checked by the data-base program for consistency and completeness and is subsequently printed in a format that can be directly pasted onto the barrel sheet for curatorial handling.

To describe sequences of rocks, the core was subdivided into lithologic units on the basis of changes in texture, grain size, mineral occurrence and abundance, rock composition, and rock clast type. For each lithologic unit and section, the following information was recorded in the database system:

1. Leg, site, hole, core number and type, and section number.
2. Unit number (consecutive downhole), position in the section, number of pieces of the same lithologic type, rock name, and identification of the describer.
3. Color of the dry rock (Munsell Soil Color Charts, 1975) and presence and character of any structural fabric.
4. Number of mineral phases visible with a hand lens and their distribution within the unit, together with the following information for each phase: (a) abundance (volume %), (b) size range in millimeters, (c) shape, (d) degree of alteration, and (e) further comments.

5. Groundmass texture: glassy, fine grained (<1 mm), medium grained (1–5 mm), or coarse grained (>5 mm). Grain-size changes within units are also noted.

6. Presence and characteristics of secondary minerals and alteration products.

7. Abundance, distribution, size, shape, and infilling material of vesicles (including the proportion of vesicles that are filled by alteration minerals).

8. Rock structure: determination of whether the flow is massive, pillowed, thin or sheetlike, brecciated, or a hyaloclastite.

9. Relative amount of rock alteration, expressed in the description. Alteration is graded as fresh (<2%), slightly altered (2%–10%), moderately altered (10%–40%), highly altered (40%–80%), very highly altered (80%–95%), and completely altered (95%–100%). The type, form, and distribution of alteration are also noted.

10. Presence of veins and fractures, including their abundance, width, mineral fillings or coatings, and orientation. The orientation of veins and fractures is measured with a protractor, such that the top of each core is considered 0°.

11. Other comments, including notes on the continuity of the unit within the core and the interrelationship of units.

Basalts and diabases are termed aphyric (<1%), sparsely phyric (1%–2%), moderately phyric (2%–10%), or highly phyric (>10%), depending upon the proportion of phenocrysts visible with a hand lens or binocular microscope. Basalts are further classified by phenocryst type (e.g., a moderately phyric olivine plagioclase basalt contains 2%–10% phenocrysts, mostly plagioclase, with subordinate olivine). Volcanic rock names were initially assigned from megascopic phenocryst assemblages. Where chemical analyses or thin sections were available, more specific rock names were given.

The descriptive terms used for basalts and diabases differ somewhat from that suggested in the "Shipboard Scientists Handbook." For phyric rocks, the mineral name modifiers to the rock name are given in order of increasing abundance in the sample. In addition, the proportion of phenocrysts (e.g., sparsely phyric) is given as the first modifier to the rock name. We also emphasize that the diabasic rocks contain a range of feldspar compositions, instead of the feldspar being limited to a labradorite composition.

Lavas erupted on the seafloor typically show a sparsely crystalline glassy margin overlying a variolitic (used here as synonymous with spherulitic) zone of quench phases, which may then grade into a coarser microlitic zone toward the interior of the flow. In many samples, these zones are not well defined and may be expressed as alternating layers or areas. Varioles commonly show a sheaflike or radial form, and microlites commonly show crystal clustering networks in areas of microlitic texture. We follow Bryan (1972) and Natland (1978) in interpreting these textures as quench-growth features rather than post-solidification phenomena. We also think that the microlitic texture occurs independently of the presence of phenocrysts.

Thin Section Descriptions

Thin sections of igneous rocks were examined to complement and refine the hand-specimen observations. The percentages and textural descriptions of the individual phases are reported in the computerized database HRTHIN. The same terminology was used for the thin section descriptions as was used for the megascopic descriptions. Thin section descriptions are included in the appendixes.

X-ray Diffraction Analysis

A Philips ADP 3520 X-ray diffractometer was used for the XRD analysis of mineral phases. Ni-filtered CuKΣ radiation generated at 40 kV and 35 mA was used. Peaks were scanned from 2° to 70° 2θ, with a step size of 0.02° and a counting time of 1 s per step.

Samples were ground to <200 mesh in either a Spex 8000 Mixer Mill (in tungsten carbide, alumina ceramic, or agate grinding containers) or an agate pestle and mortar. The powder was then pressed into the sample holders or smeared onto glass plates for analysis. Diffractograms were interpreted with the help of a computerized search and match routine using the Joint Committee on Powder Diffraction Standards powder files.

X-ray Fluorescence Analysis

Before undergoing X-ray fluorescence (XRF) analyses, samples were sawn into small blocks and the saw marks and exterior surfaces (with any associated contamination) were removed by grinding on a diamond lap. The sample blocks were rinsed in deionized water and dried. The cleaned blocks were then crushed in a Spex 8510 shatterbox using tungsten carbide or alumina ceramic barrels. Where recovery permitted, at least 20 cm^3 of material was ground to ensure representation of the sample. The tungsten carbide barrel introduces considerable W contamination and minor Ta and Co contamination, resulting in the powder becoming unsuitable for instrumental neutron activation (INNA) analysis. Sample Nb contamination resulting from grinding in the tungsten carbide barrel has been determined to be below 1 ppm (D. Sims, pers. comm., 1990).

A fully automated wavelength-dispersive ARL8420 XRF (3 kW) system equipped with an Rh target X-ray tube was used to determine the major oxide and trace element abundances of whole-rock samples. Analyses of the major oxides were carried out on lithium borate glass disks doped with lanthanum as a "heavy absorber" (Norrish and Hutton, 1969). The disks were prepared from 500 mg of rock powder that had been ignited for 2 hr at about 1030°C and mixed with 6.0 g of preweighed (on shore) dry flux consisting of 80% lithium tetraborate and 20% La_2O_3. This mixture was then melted in air at 1150°C in a Pt-Au crucible for about 10 min and poured into a Pt-Au mold using a Claisse Fluxer. The 12:1 flux to sample ratio and the use of the lanthanum absorber made matrix effects insignificant over the normal range of igneous rock compositions. Hence, the relationship between X-ray intensity and concentration becomes linear and can be described by

$$C_i = I_i \times m_i) - b_i,$$

where C_i = concentration (wt%) of oxide i, I_i = net peak intensity (cps) of oxide i, m_i = slope of calibration curve (wt%/cps) for oxide i, and b_i = measured blank (wt%) of oxide i (wt%).

The slope m_i was calculated from a calibration curve derived from the measurement of well-analyzed reference rocks (BHVO-1, G-2, AGV-1, JGB-1, JP-1, BR, and DRN). Analyses of common standards derived from the calibration curves used are given in Table 3. The blank b_i was determined by regression analysis from the calibration curves.

Systematic errors resulting from short- or long-term fluctuations in X-ray tube intensity and instrument temperature were addressed by counting an internal standard between no more than six unknowns in any given run. The intensities of this standard were normalized to its known values, providing correction factors to the measured intensities of the unknowns. To reduce shipboard weighing errors, two glass disks were prepared for each sample. Accurate weighing was difficult on board the moving platform of *JOIDES Resolution* and was performed with particular care as weighing errors could be a major source of imprecision in the final analysis. Loss on ignition was determined by drying the sample

Table 3. XRF analyses of standards derived from the calibrations used for whole-rock analysis.

	BHVO[1]			AII-92-26			UBN		K1919		
	Published values	Leg 135		Published values	Leg 135		Published values	Leg 135	Published values	Leg 135	
SiO_2	49.62	50.02	49.86	49.34	49.2	49.68	44.73	45.03	49.73	50.09	49.93
TiO_2	2.68	2.76	2.76	1.75	1.74	1.75	0.13	0.13	2.83	2.77	2.75
Al_2O_3	13.67		13.67	15.49		15.69	3.3	3.52	13. 75	13.6	13.63
Fe_2O_3	12.23	12.38	12.42	10.85	10.7	11.03	9.5	9.83	12.21	12.32	12.04
MnO	0.17	0.17	0.17	0.18	0.17	0.18	0.14	0.15	0.18	0.17	0.17
MgO	7.21	7.25	7.44	7.51	7.52	7.62	40.12	40.97	6.83	6.95	6.96
CaO	11.32	11.42	11.41	11.16	10.86	11.03	1.36	1.43	11.32	11.4	11.27
Na_2O	2.17	2.33	2.46	3.07	3.24	3.14		0.48	2.35	2.4	2.4
K_2O	0.53	0.53	0.54	0.17	0.18	0.17	0.05	0.02	0.53	0.54	0.53
P_2O_5	0.27		0.28	0.16		0.17	0.05	0.02	0.28	0.27	0.27
Total	99.87		101.01	99.68		100.46	99.38	101.58	100.01	100.51	99.95

at 110°C for 8 hr and then weighing before and after ignition at 1030°C in air.

Trace element determinations were made on pressed-powder pellets prepared by pressing (with 7 tons of pressure) a mixture of 5.0 g of dry rock powder (dried at 110°C for >2 hr) and 30 drops of polyvinyl alcohol binder into an aluminum cap. A modified Compton scattering technique based on the intensity of the Rh Compton peak was used for matrix absorption corrections (Reynolds, 1967).

Replicate analyses of the rock standards show that the major element data are precise within 0.5% to 2.5%, and are considered accurate to ≈1% for Si, Ti, Fe, Ca, and K and between 3% and 5% for Al, Mn, Na, and P. The trace element data are considered accurate between 2% and 3% or 1 ppm (whichever is greater) for Rb, Sr, Y, and Zr and between 5% and 10% or 1 ppm for the others. The accuracy of Ba and Ce is considerably less, and they are reported primarily for purposes of internal comparison. Analytical conditions for the XRF analyses are given in Table 4.

Means and standard deviations of analyses of K1919-B and BHVO run throughout Leg 135 are shown in Table 5. Precision is <3% for SiO_2, MgO, and K_2O; <6% for MnO and P_2O_5; <1% for Fe_2O_3, Al_2O_3, and CaO; <2% for Nb, Y, Sr, Zn, Cu, and Ni; <4% for Zr; <6% for V and Rb; and <10% for Ba and Ce. SiO_2 values showed a systematic 0.9 wt% (absolute) increase in analyses for Sites 840 and 841. Ba is systematically about 20% too high and Zr 7% too high compared with recommended values for BHVO.

PHYSICAL PROPERTIES

The shipboard measurement of physical properties of the materials sampled during drilling provides information that can aid in the characterization of different lithologic units, allows comparison to and verification of the downhole logging results, and provides important constraints on the interpretation of seismic-reflection and other geophysical data. The physical properties data are also used to estimate permeability and the degree of consolidation, to correct sedimentation rates, and to aid in heat-flow calculations.

On Leg 135, the physical properties measured were index properties, compressional wave (*P*-wave) sonic velocity, undrained vane shear strength, and thermal conductivity. The physical properties measured aboard *JOIDES Resolution* are defined as follows:

1. Index properties: determinations of bulk density, grain density, porosity, water content, and void ratio measured by gamma-ray attenuation techniques (GRAPE) and by gravimetric techniques.

2. Compressional sonic velocity: the speed of a compressional acoustic wave through sediments or rocks in which the velocity is determined by measuring the traveltime of a 500-kHz wave through a measured distance in either or both vertical and horizontal directions on the recovered core.

3. Vane shear strength: a relative indicator of the shear strength of undrained clay sediments, determined by measuring the resistance of the sediment to loads.

4. Thermal conductivity: the ability of sediment or rocks to transport heat, determined by heating sediment or rocks with a probe and monitoring the change in temperature over time.

5. Temperature measurements: temperature measurements were made with the water sampler temperature probe (WSTP) in sediments at discrete points ahead of the drill bit during drilling. These measurements are used to give a geothermal gradient, and when calibrated with the measured thermal conductivity measurements, an estimation of heat flow.

A discussion of the physical property determinations with respect to equipment, methods, errors, correction factors, and problems related to coring disturbance is presented by Boyce (1973, 1976). Physical properties are influenced by drilling and sample disturbance, and by the testing procedures used in the laboratory. For example, the water content of a particular sample can be affected during drilling when the drilling-disturbed core may be surrounded by the drilling fluid (seawater) for many hours and in the laboratory after core splitting, when the sample may dry out.

Samples for physical properties determinations were selected from the areas of least core disturbance, and sufficient samples were tested to allow for the characterization of all major lithologic units. Typically, a discrete sample was selected for index properties evaluation from at least every other core section for full cores and from every core section for short cores.

Compressional wave velocities were normally taken on the same samples or on samples taken adjacent to the index properties samples. Samples were taken to be representative of the cored section as a whole; however, some samples were taken from thin layers of markedly different lithologies within a core or section, such as carbonate-rich layers or thin turbidite deposits within a nannofossil ooze. Sample selection and frequency depended on the thickness and homogeneity of a particular sequence.

The testing methods employed during Leg 135 are as follows. Sample processing aboard ship was performed in the order given here. First, after acquisition, the cores were allowed to equilibrate thermally on board for 4 hr. After equilibration, cores that completely fill the core liner were sent through the gamma-ray attenuation porosity evaluator (GRAPE) and compressional wave logger (*P*-wave logger), and soft-sediment thermal conductivity determinations were made on selected sections of the whole core as appropriate. Following core splitting, vane shear analyses were performed on clay sediment cores, velocity measurements were

Table 4. Leg 135 XRF analytical conditions.

Element	Line	Crystal	Detector	Collimator	Peak angle (degrees)	Background offset (degrees)	Total count time (s)	
							Peak	Background
SiO_2	K	PET(002)	FPC	Coarse	109.10	0	40	0
TiO_2	K	LiF(200)	FPC	Fine	86.16	0	40	0
Al_2O_3	K	PET(002)	FPC	Coarse	144.49	0	100	0
Fe_2O_3*	K	LiF(200)	FPC	Fine	57.53	0	40	0
MnO	K	LiF(200)	KrSC	Fine	63.03	0	40	0
MgO	K	TLAP	FPC	Coarse	44.88	±0.80	200	400
CaO	K	LiF(200)	FPC	Coarse	113.18	0	40	0
Na_2O	K	TLAP	FPC	Coarse	54.73	−1.20	200	200
K_2O	K	LiF(200)	FPC	Fine	136.66	0	40	0
P_2O_5	K	Ge(111)	FPC	Coarse	141.00	0	100	0
Rb	K	LiF(200)	Scint	Fine	18.60	0	100	0
Nb	K	LiF(200)	Scint	Fine	21.39	±0.35	200	200
Zr	K	LiF(200)	Scint	Fine	22.54	±0.35	100	100
Y	K	LiF(200)	Scint	Fine	23.83	±0.40	100	100
Sr	K	LiF(200)	Scint	Fine	25.15	±0.41	100	100
Rb	K	LiF(200)	Scint	Fine	26.60	±0.60	100	100
Zn	K	LiF(200)	Scint	Fine	41.81	±0.40	60	0
Cu	K	LiF(200)	Scint	Fine	45.02	±0.40	60	60
Ni	K	LiF(200)	Scint	Coarse	48.64	±0.60	60	60
Cr	K	LiF(200)	FPC	Fine	69.38	±0.50	60	60
Fe	K	LiF(220)	FPC	Fine	85.73	−0.40 ± 0.70	40	40
V	K	LiF(220)	FPC	Fine	123.20	−0.50	60	60
TiO_2	K	LiF(200)	FPC	Fine	86.16	±0.50	40	40
Ce	L	LiF(220)	FPC	Coarse	128.35	±1.50	100	100
Ba	Lβ	LiF(220)	FPC	Coarse	128.93	±1.50	100	100

All elements analyzed under vacuum on goniometer 2, at generator settings of 60 kV and 50 mA. Total Fe as Fe_2O_3. ± = background offset above and below peak 2Ø. FPC = flow proportional counter using P_{10} gas, KrSC = sealed Krypton gas counter, and Scint: NaI scintillation counter.

Table 5. Replicate analyses of K1919-B (major elements) and BHVO (trace elements) from Leg 135.

	Recommended value	Cumulative		Site 834		Sites 835 and 837		Site 836		Site 839		Sites 840 and 841	
		Mean	SD	Mean	SD	Mean	SD	Mean	SD	Mean	SD	Mean	SD
SiO_2	49.73	49.67	0.85	49.70	0.24	49.37	0.17	49.68	0.46	49.72	0.17	50.49	0.16
TiO_2	2.83	2.78	0.07	2.77	0.07	2.84	0.13	2.76	0.01	2.76	0.01	2.76	0.01
Al_2O_3	13.75	13.58	0.07	13.60	0.07	13.61	0.07	13.58	0.04	13.56	0.05	13.53	0.08
Fe_2O_3	12.21	12.02	0.03	12.01	0.04	12.02	0.02	12.02	0.05	12.02	0.02	12.04	0.01
MnO	0.18	0.16	0.01	0.16	0.01	0.17	0.00	0.16	0.01	0.16	0.01	0.17	0
MgO	6.83	6.91	0.08	6.91	0.08	6.92	0.08	6.82	0.15	6.91	0.07	6.96	0.04
CaO	11.32	11.29	0.03	11.28	0.03	11.29	0.04	11.32	0.08	11.30	0.03	11.30	0.02
Na_2O	2.35	2.45	0.05	2.42	0.03	2.43	0.02	2.44	0.08	2.49	0.04	2.46	0.05
K_2O	0.53	0.54	0.01	0.54	0.01	0.55	0.01	0.54	0	0.54	0.01	0.54	0
P_2O_5	0.28	0.28	0.01	0.27	0.01	0.29	0.02	0.28	0.01	0.28	0.01	0.29	0.01
N		32		11		5		2		8		6	
Nb	19.0	19.1	0.3	19.2	0.4	19.0	0	19.0	—	19.0	0	19.3	0.6
Zr	180	192	7	187	13	193	1	193	—	194	1	196	1
Y	26.0	26.5	0.5	26.6	0.5	27.0	0	27.0	—	26.3	0.5	26	0
Sr	420	392	3	393	1	393	2	397	—	390	4	390	1
Rb	10.0	9.0	0.4	9.0	0	9	6	9	—	9	0.8	9	0
Zn	113	109	2	109	2	109	2	109	—	108	2	109	1
Cu	140	135	2	136	2	136	1	136	—	135	3	134	1
Ni	120	122	2	121	1	120	5	122	—	122	1	123	2
Cr	306	290	8	291	8	290	12	303	—	284	6	292	6
V	310	315	20	320	4	332	34	324	—	304	8	296	3
Ce	38	35	4	37	4	37	5	32	—	32	2	32	4
Ba	127.0	155.0	9.0	147.0	11.0	15.6	5.0	172.0	—	160.0	4.0	155.0	9.0
		17		5		4		1		4		3	

Note: Oxides in weight percent, trace elements in ppm. SD = standard deviation and *N* = numbers of samples.

made through the split core and core liner for unconsolidated sediments and on discrete samples otherwise, and samples were taken from the working half of the split core for index properties determinations and for thermal conductivity measurements on lithified sediments or igneous rocks.

Index Properties Determinations

Gamma-ray Attenuation Porosity Evaluator

The GRAPE technique was described by Boyce (1976). This method makes nondestructive, continuous measurements of wet-bulk density on whole APC and XCB cores or on discrete samples by comparing the attenuation of gamma rays through the cores and samples with attenuation through an aluminum or quartz standard (Boyce, 1976). In continuous GRAPE mode, APC cores and the first few XCB cores were measured; untested XCB cores retained a large air-space around the recovered core, and the GRAPE is calibrated for full-diameter core only. Aluminum, quartz, and water standards were used for calibration of the apparatus at least once a day. After the recovered cores were cut into 1.5-m sections and allowed to equilibrate to laboratory temperature, the individual sections were placed horizontally on the multisensor track (MST) and moved on a conveyor belt through the GRAPE, *P*-wave logger, and magnetic susceptibility sensors. The attenuation of the gamma rays passing through the liner and core was measured every 2 cm, and the bulk density was calculated from the attenuation values. The GRAPE data were then filtered to remove values that resulted from the presence of gas, gaps, and end-cap effects before the data were averaged over 0.2- to 0.5-cm intervals. All bulk-density data are reported in units of g/cm^3. The GRAPE was not used to measure highly disturbed material or biscuited material in rotary-drilled cores.

The GRAPE was also used in a noncontinuous mode on individual samples, with gamma-ray attenuation measured over a 2-min period through a sample followed by a similar 2-min count through air and a quartz standard to determine the bulk density (Boyce, 1976). Basalt samples taken for velocity analysis were also run through a 2-min GRAPE analysis.

Gravimetric Determination of Index Properties

Destructive index properties determinations on discrete samples were calculated from careful measurements of wet and dry weights and wet and dry volumes on 10–20 cm^3 of sediment or rock according to procedures referenced in American Society of Testing and Materials (ASTM, 1989) and determined for Leg 131 (Shipboard Scientific Party, in press). Index properties samples (from at least every other section for full core recovery, and at least one per core in low-recovery intervals) for the analysis of wet- and dry-bulk density, water content, grain density, and porosity were taken immediately adjacent (within a 2–10-cm interval) to measurements of sonic velocity and undrained vane shear strength. Each sample was placed in a small aluminum beaker and weighed, with a precision of about 0.02 g, using a calibrated Scientech 202 electronic balance. Wet volumes were measured using a Quantochrome Helium Penta-Pycnometer. The sample was then oven dried at 110° ± 5°C for 24 hr (ASTM, 1989). Dry weights and volumes were then measured with the same balance and pycnometer. An additional step was necessary for small basalt density samples taken adjacent to the velocity and 2-min GRAPE basalt cubes. These basalt samples were weighed and then powdered so that the volume of material could be obtained in the pycnometer.

The equations used by the ODP database to calculate index properties are contained in Boyce (1976) and Shipboard Scientific Party (in press). The definitions and units used for the index properties are

1. porosity (%) = 100 · volume of water/volume of wet sediment;
2. bulk density (g/cm^3) = weight of wet sediment/volume of wet sediment;
3. grain density (g/cm^3) = weight of dry sediment/volume of dry sediment;
4. water content (%) = 100 ≈ weight of water/dry weight of sediment; and
5. void ratio (unitless) = volume of water/volume of dry sediment.

Salinity-corrected physical properties were computed for all samples by assuming a pore-water salinity of 35‰, and by subtracting the estimated weight and volume of the residual salt.

As a further check on shipboard grain-density measurements, approximately 20–30 cm^3 of wet material was occasionally taken and preserved for later shore-based specific gravity testing at ODP using an ASTM-approved water pycnometer. These special physical properties samples (10–15 total) were selected at the sampling table from representative lithologies and from sample locations adjacent to the locations of the normal index properties samples so that the results of the specific gravity tests could be compared directly.

Sonic Velocities

P-wave Velocity Logger

The *P*-wave logger was operated simultaneously with the GRAPE because both are mounted on the same frame. A short 500-kHz compressional wave pulse was produced by a transducer at a repetition rate of 1 kHz. A receiving transducer was positioned such that the two transducers were aligned perpendicular to the core axis. A pair of displacement transducers monitor the separation between the compressional wave transducers, which allows for variation in the outside liner diameter without degrading the accuracy of the velocities. Measurements were taken at 2.0-cm intervals as the core moved past the transducer. The *P*-wave logger was calibrated with seawater and aluminum as standards at least once per drill site.

Water was applied to the core liner to improve the acoustic contact between the transducers and the liner. As with the GRAPE, only APC and the first few XCB cores were measured because good quality data can be obtained only on core that completely fills the liner. The deeper XCB cores and all RCB cores had annular voids present between the core and the inside of the liner, which prevented transmission of the compressional waves between the transducers. The *P*-wave logger data were filtered to remove data that were the result of gas, gaps and end-cap effects. Additional filtering was performed to eliminate data with a signal strength below a threshold value of 200 signal strength units. Finally, the data were averaged over 0.2- or 0.5-cm intervals before the figures were plotted.

Hamilton Frame Velocimeter

The Hamilton Frame Velocimeter is connected to a Tektronix DC 5010 counter/timer and sends a 500-kHz compressional wave through a measured thickness of sample. The sample thickness was measured by using a variable resistor attached to the calipers that hold the sample between the transducers on the Hamilton Frame. The Hamilton Frame transducers and calipers were calibrated with lucite and aluminum standards of known velocity and thickness. Zero times were calculated by measuring the velocity through a series of aluminum and lucite standards of known thickness and velocity, and then performing a linear regression on the resulting traveltime vs. distance data. The thickness and zero-

time corrections were applied to the data, and the compressional velocity was then calculated by

velocity = thickness of sample/traveltime through sample.

All velocity data are reported in units of m/s.

Samples for velocity measurements were selected from the most intact portions of the core sections, avoiding the top and bottom of the core and other areas with obvious or severe drilling disturbance. If core disturbance was so severe as to preclude intact samples, velocity measurements were not made in that core. Samples were cut from soft sediment with either a small (about 20 cm) parallel-sided scoop or with a knife blade or spatula, with attention paid to obtain flat, parallel faces on the sample. In hard rocks and basalt, samples were obtained using a double-bladed diamond saw (about 1.5-cm separation). Where either of these techniques was not possible because of unconsolidated, soft, soupy, or very friable sediments, velocity was measured in the Hamilton Frame perpendicular to the core through the core liner (C direction), and a correction was applied for the effects of the liner. Velocities were measured on at least every other section, or about three to four measurements per full core, with additional velocity measurements taken of varying lithologies within a core. Seawater was used to improve the acoustic contact between the sample and the transducers. Routinely, velocity and index properties samples were taken from adjacent positions in the core.

The treatment of basalt or hard-rock samples for velocity analysis was handled somewhat differently. A cube about 1.5 cm on a side was cut using the double-bladed rock saw, and, if the orientation was known, velocity determinations were made in all three directions of the core (A, along the core axis; B, across the core parallel to the split face; and C, across the core perpendicular to the cut face) to determine velocity anisotropy (vertical vs. horizontal) within the cored materials. On basalt samples, three velocity determinations were made across each face of the sample, and the resulting average reported as the velocity in each direction. These cubes were also used for 2-min GRAPE analysis to determine the bulk density.

Thermal Conductivity

Thermal conductivity was measured with needle probes containing heater wires and calibrated thermistors connected to a Thermcon-85 unit. Before thermal conductivity was measured, the cores were allowed to equilibrate at room temperature for at least 4 hr, and were run through the GRAPE and *P*-wave logger. Then, thermal equilibrium was determined by requiring that thermal drift in the core before any measurements were obtained be <0.004°C/min. Each needle also had a correction factor based on calibration for the difference between measured and true thermal conductivities, as determined from a series of tests with standards of known conductivities for each probe needle. The thermal conductivity techniques used, either "full-space" measurements in soft sediments or "half-space" in lithified or basalt rocks, are described by Von Herzen and Maxwell (1959) and Vacquier (1985). All thermal conductivity data are reported in units of W/(m · °K) and have an estimated error of 5%–10%.

Soft-sediment Thermal Conductivity

Up to four needle probes were inserted into full sediment cores (commonly Sections 2, 3, 4, and 6) through holes drilled into the unsplit core liner. An additional probe was inserted into a reference material to monitor the probe behavior. Probe locations were carefully positioned where visual examination of the core, and the GRAPE and sonic velocity measurements, indicated a uniform sample completely filling the core liner. The instrument first monitored thermal drift within the core. Once the temperature had stabilized, the probes were heated, and the coefficient of thermal conductivity was calculated as a function of the change in resistance in the probe about every 20 s over a 6-min interval. When the sediment became too stiff to allow easy insertion of the probe, holes were drilled into the core material before inserting the probes or, more commonly, pieces of the cut core were measured using the "half-space" method. All measurements were calibrated for thermal drift before heat was applied.

Hard-rock Thermal Conductivity

Thermal conductivity measurements on well-lithified sediments and rock were conducted on split cores with the use of a needle probe partially embedded in a slab of insulating material. The flat surface of a selected sample of split core was polished with fine sandpaper and then placed on top of the slab. Type 120 Thermal Joint Compound from EG&G Wakefield Engineering was used to improve the thermal contact between the slab and the sample. The sample and the slab were immersed in a saltwater bath and allowed to reach thermal equilibrium with the water. The probe was heated, and measurements of resistance change in the probe were made every 9 s for a 6-min interval. The thermal conductivity was determined from the most linear portion of a temperature vs. log-time plot.

Undrained Vane Shear Strength

The undrained vane shear strength of the sediment, as described by Boyce (1977) and Lee (1984), was determined by means of a Wykeham-Farrance motorized vane apparatus that used a four-bladed vane with a diameter of 1.28 cm and a length of 1.28 cm. The vane was inserted into the split core section perpendicular to its face (i.e., perpendicular to the core axis), to a point where the top of the blade was covered. The vane was then rotated at a rate of about 90°/min until the sediment failed. The undrained shear strength was calculated from the peak torque obtained at failure. Vane testing was suspended when radial cracking or other noncylindrical failure surfaces developed around the vane. The noncylindrical failures were observed in stiff sediments that had values of undrained shear strength exceeding approximately 100 kPa. All shear strength values are reported in units of kPa.

Post-testing Data Presentation

GRAPE, *P*-wave logger, thermal conductivity, and all physical properties data measured on discrete samples were entered into the shipboard physical properties data collection system. The GRAPE and *P*-wave logger data were filtered, edited, and blocked to remove spurious data caused by highly disturbed cores, voids, or section ends and to reduce the number of data points. The data-collection system computes the depth below seafloor, index properties, shear strength, and velocities for each sample, as appropriate.

The physical properties collected for samples during Leg 135 are presented in each site chapter. All measurements of index properties, shear strength, thermal conductivity, and Hamilton Frame velocity data made on discrete samples are presented in tables as well as in figures. However, the GRAPE and *P*-wave logger data are presented only in figure form as the number of data points would generate excessively long tables.

Temperature Measurements

The water sample temperature probe (WSTP) (Yokota et al., 1979) was used to make temperature measurements in the sedimentary sections at each site. The probe is pushed into sediments ahead of the drill bit during drilling operations through unconsolidated and semiconsolidated sediments. Temperature measurements are used to determine the vertical temperature gradients in

the sediments and are used together with measurements of thermal conductivity to determine heat flow through the seafloor (Hyndman et al., 1987). After inserting the probe into the sediments, the temperature history in the sedimentary section should be such that after 5 min in the sediment, the decay curve should be approximated by

$$T(t) = A/t + T_{eq},$$

where A is a constant determined experimentally, t is time, and T_{eq} is the equilibrium formation temperature. The equilibrium temperatures of several probes can be plotted vs. depth to yield a temperature gradient.

DOWNHOLE MEASUREMENTS

Tool Strings

Downhole logs can be used to characterize the geophysical, geochemical, and structural properties of a drilled sequence. Log measurements have an advantage over core-based measurements in that log measurements represent continuous and *in situ* measurements of the borehole. After coring is completed at a hole, a tool string is lowered downhole on a seven-conductor cable, and each of several tools in the tool string continuously monitors some property of the adjacent borehole. Three Schlumberger tool strings were used on Leg 135: the Quad tool (and variations of the Quad tool: the seismic stratigraphic and lithoporosity tool strings), geochemical tool string, and the formation microscanner (FMS) string. The Lamont-Doherty temperature tool was attached to the base of the Schlumberger tool strings. The analog borehole televiewer (BHTV) was used at selected sites; although the digital BHTV was aboard ship, it was not used because of electronic malfunctions.

The Quad-tool combination used on Leg 135 comprised a digital string, consisting of long-spaced sonic transducer/receiver with a digital sonic cartridge (LSS/SDT), high-temperature lithodensity tool (HLDT), dual induction tool (DIT), compensated neutron porosity tool (CNT), mechanical caliper (MCD), and natural gamma-ray tool (NGT). This tool combination measures compressional wave velocity and provides indicators of the two variables that most commonly control velocity: porosity, as indicated by density or resistivity, and clay content, as indicated by the natural gamma tool. The Quad-tool combination can be broken down into two strings: the seismic stratigraphic combination and the lithoporosity combination. The seismic stratigraphic string comprises the LSS/SDT, DIT, and NGT. The lithoporosity string combines the HLDT, CNT, and NGT. A caliper device is present on all of these tool strings.

The geochemical tool combination for Leg 135 consists of the NGT, an aluminum clay tool (ACT), a gamma-ray spectrometry tool (GST), a compensated neutron porosity tool (CNT), and a caliper. This tool string measures the relative concentrations of 12 elements: silicon, calcium, aluminum, iron, titanium, sulfur, hydrogen, chlorine, potassium, thorium, uranium, and gadolinium.

The FMS tool string includes both the FMS and a general purpose inclinometer tool (GPIT) that spatially orients the FMS resistivity image of the borehole wall. The tool string also contains an NGT to allow depth correlation of the FMS data with other logs.

Logs

A brief description of logging tools run during Leg 135 is given in the following sections. A more detailed description of logging tool principles and applications is provided in Schlumberger (1989), Serra (1984, 1989), and Timur and Toksöz (1985).

Electrical Resistivity

The DIT provides three different measurements of electrical resistivity, each capable of penetrating a different depth into the borehole wall. Two induction devices (deep and medium resistivity) send high-frequency alternating currents through transmitter coils, creating magnetic fields that induce secondary (Foucault) currents in the formation. These ground-loop currents produce new inductive signals, proportional to the conductivity of the formation, which are recorded by the receiving coils. Measured conductivities then are converted to resistivity. A third device (spherically focused resistivity) measures the current necessary to maintain a constant voltage drop across a fixed interval. Vertical resolution is about 2 m for the medium and deep resistivity devices and about 1 m for the focused resistivity.

Water content and salinity are by far the most important factors controlling the electrical resistivity of rocks. To a first order, resistivity responds to the inverse square root of porosity (Archie, 1942). Other factors influencing resistivity include the concentration of hydrous and metallic minerals, vesicularity, and the geometry of interconnected pore space.

Sonic Velocity

The long-spaced sonic (LSS) tool uses two acoustic transmitters and two receivers to measure the time required for sound waves to travel over source-receiver distances of 2.4, 3.0, and 3.6 m. The raw data are processed to give the time required for a sound wave to travel through 0.31 m of formation; these traveltimes are then converted to sonic velocities. Values below 1.45 km/s and above 7.62 km/s are excluded. First arrivals for the individual source-receiver paths are used to calculate the velocities of the different waves travelling in the formation (compressional, shear, etc.). Only compressional wave velocity is determined during data acquisition, but waveforms are recorded for post-cruise determination of shear wave velocities and, possibly, improved compressional wave velocities. The vertical resolution of the tool is 0.61 m. Compressional wave velocity is controlled dominantly by porosity and lithification; decreases in porosity and increases in lithification cause the velocity to increase.

The sonic tool is commonly used as part of the Quad-tool combination. Ideally, the sonic tool is used alone, as the shorter seismic string can be centralized in the borehole by means of a three-arm caliper that is eliminated on the Quad-tool for reasons of space. When the sonic tool is centered, better velocity data are collected because sonic pulses are radiated symmetrically. Also, the tool firing time can be higher, allowing greater signal strength, better signal reception, and less cycle skipping caused by weak signal strengths.

Natural Gamma Ray

The natural gamma-ray tool (NGT) measures the natural radioactivity of the formation. Most gamma rays are emitted by the radioactive isotope ^{40}K and by the radioactive elements of the U and Th series. The gamma-ray radiation originating in the formation close to the borehole wall is measured by a scintillation detector mounted inside the sonde. The analysis is achieved by subdividing the entire incident gamma-ray spectrum into five discrete energy windows. The total counts recorded in each window, for a specified depth in the borehole, are processed to give the elemental abundances of K, U, and Th.

Because radioactive elements tend to be more abundant in clay minerals relative to other common sedimentary minerals, the gamma-ray curve is commonly used to estimate the clay or shale content. Other rock or sediment types may also have radioactivity values ranging from moderate to extremely high, because of the presence of volcanic ash, potassium feldspar, or other radioiso-

tope-containing minerals. The measurement is also sensitive to hole size, drilling, mud density (if mud is used), and formation bulk density. Post-cruise processing can correct for borehole size and mud density. An NGT is carried on all tool strings for use as a cross-correlation tool between logging runs.

Lithodensity Tool

The high-temperature lithodensity tool (HLDT) uses a ^{137}Ce gamma-ray source and measures the resulting flux at fixed distances from the source. Under normal operating conditions, attenuation of gamma rays is caused chiefly by Compton scattering (Dewen, 1983). Formation density is extrapolated from this energy flux by assuming that the atomic weight of most rock-forming elements is approximately twice the atomic number. A photoelectric effect index is also provided. Photoelectric absorption occurs in the energy window below 150 keV and depends on the energy of the incident gamma ray, the atomic cross section, and the nature of the atom. Because this measurement is almost independent of porosity, it can be used directly as an indicator of matrix lithology. The radioactive source and detector array are placed in a tool that is pressed against the borehole wall by a strong spring arm; the position of this spring arm indicates hole diameter. Excessive roughness of the hole will cause some drilling fluid to infiltrate between the skid and the formation. As a consequence, density readings can be artificially low. Approximate corrections can be applied by using caliper data. The vertical resolution is about 0.30 m.

Compensated Neutron Porosity

A radioactive source mounted on the compensated neutron porosity (CNT) sonde emits fast neutrons (4 MeV) into the formation, where they are scattered and slowed by collisions with other nuclei. When the neutrons reach a low energy level (0.025 MeV) they are captured and absorbed by atomic nuclei such as hydrogen, chlorine, silicon, and boron. The scattering cross section is the quantity that describes the rate at which neutrons are slowed. Because the scattering cross section for hydrogen is about 100 times larger than for any other common element in the crust, most energy dissipation is caused by collisions with water molecules. Therefore, a change in the number of neutrons detected at a receiver can be related to porosity. In practice, an array of detectors is used to minimize hole size or drilling fluid effects. Because water is present both in pores and as bound water (e.g., clay minerals), porosity measurements made in the presence of hydrous minerals are overestimates of the true porosity. The vertical resolution of the tool is theoretically about 0.25 m, but a low signal-to-noise ratio degrades this potential resolution.

Caliper Devices

Caliper logs record the diameter of the hole and are useful in evaluating whether information from the logs is valid and in providing data for post-cruise log correction routines. If the hole diameter exceeds the maximum extension of the calipers, then the data acquired during that interval may be in error. Calipers are run on each tool string to measure the hole diameter, to centralize the tool string, or to hold tool pads against the borehole wall.

The MCD run on the seismic stratigraphic string provides a two-dimensional caliper log of the borehole by means of a bow-spring-mounted measurement system. The caliper's main use is to provide tool centralization for the sonic log. Areas where the hole is too wide for the caliper to centralize the sonic tool may recover sonic data characterized by weak signals or by cycle skipping. The caliper tool is subject to sticking when formation mud gets into its mechanical parts, resulting in bimodal (fully open or nearly fully closed) readings.

The hole diameter (HD) caliper is run with the lithodensity tool and gives the largest measure of hole diameter (about 48 cm, or 19 in.). The HD caliper is useful for detecting washouts or constrictions, and is also mechanically more reliable than the MCD caliper. If the hole diameter exceeds 48 cm, values from density and neutron porosity curves may be erroneous. Post-cruise corrections for poor pad contact can be made with a density compensation factor, but when the correction values are large, the compensation may be only approximate.

Calipers on the FMS tool give hole diameter and ellipticity information from four arms. Thus, the FMS caliper gives the most accurate and detailed hole information. The FMS calipers reach their maximum extension at 39.4 cm (15.5 in.), and holes larger than this will not be imaged well by the FMS tool, as the FMS pads will not make proper contact with the hole wall.

Gamma-ray Spectrometry Tool

The induced gamma-ray spectrometry tool consists of a pulsed source of 14-MeV neutrons and a gamma-ray scintillation detector. A shipboard computer performs spectral analysis of gamma rays resulting from the interactions of neutrons emitted by the source with atomic nuclei in the formation (Hertzog, 1979). Characteristic sets of gamma rays from six elements dominate the spectrum, permitting calculation of the yields from six elements: Ca, Si, Fe, Cl, H, and S. The tool normalizes their sum, so they do not reflect the actual composition but only relative abundances of these elements. Therefore, ratios of these yields are commonly used in interpreting the lithology, porosity, and salinity of the formation fluid. Shore-based processing is used to derive actual elemental abundances from this and the other logs.

Aluminum Clay Tool

Aluminum abundance as measured by the aluminum clay tool (ACT) is determined by neutron-induced (Cf nuclear source), late gamma-ray spectrometry. By placing NaI detectors above and below the neutron source, contributions from natural gamma-ray activity can be removed. Calibration to elemental weight percent is done by taking irradiated core samples of known volume and density and measuring their gamma-ray output while being placed in a jig attached to the logging tool. This is generally done after logging.

Formation Microscanner

The formation microscanner (FMS) produces high-resolution microresistivity images of the borehole wall that can be used for making detailed sedimentological or structural interpretations and for determining the orientation of fractures and breakouts. The tool consists of 16 electrode "buttons" on each of four orthogonal pads that are pressed against the borehole wall. The electrodes are spaced about 2.5 mm apart and are arranged in two diagonally offset rows of eight electrodes each. The focused current that flows from the buttons is recorded as a series of curves that reflect the microresistivity variations of the formation. Shipboard or shore-based processing converts the current intensity measurements into gray-scale, spatially oriented images.

After acquisition, the FMS data are first shifted to meters below sea floor. Additional depth correction is done to account for the offset of each row of buttons. Magnetometer outputs are used to compute borehole and tool inclinometry, which are then used to orient images. A speed correction is made using information from the accelerometer data. To correct for offset and gain differences between buttons, goal-seeking algorithms are applied to the resistivity data sets to achieve comparable mean and standard deviations on the resistivity values seen by each button over the entire formation. Finally, image plots are generated using a

histogram equalization method to choose gray-scale class limits for the interval to be plotted. These are calculated using the resistivity values over that particular depth range. Because they are not absolute values, the gray scale for one plot may not indicate the same resistivities as the gray scale for another plot. When the diameter of the hole is greater than 39.4 cm (15.5 in.), the FMS pads do not make sufficient contact with the borehole walls to produce images of satisfactory quality.

Applications of the FMS images include the detailed correlation of coring and logging depths; orientation of cores; mapping of fractures, faults, foliations, and formation structures; and determination of strikes and dips of bedding. An important limitation is the restriction of the hole diameter to less than 41 cm (16 in.); thus, little useful information can be obtained from washed-out hole sections. FMS images are presented on microfiche at the back of this volume.

FMS Dipmeter Information

In addition to gray-scale images, FMS data can also be processed via one or more Schlumberger programs to yield a dipmeter plot (Schlumberger, 1986). Of the several types of dipmeter processing available, mean square dip (MSD) is most commonly used and is recommended as most suitable for structural work.

MSD dipmeter processing (Schlumberger, 1986) searches successive windows of the microresistivity curve from each of the four pads of the FMS tool for intervals that have a high correlation to nearby intervals on the microresistivity curves from the other three pads. After an iterative algorithm is used to find the best-fit plane through the correlation interval, the displacement of the resulting plane from the horizontal is interpreted as the apparent dip of bedding over that interval. The size of the correlation window, the percent overlap of successive windows, and other processing parameters are specified at the time of dipmeter processing. These parameters significantly affect the frequency and placement of picked dips on the final dipmeter plot, but do not have as significant an effect on the interpreted dip angle and direction. The dipmeter processing for Leg 135 employed Schlumberger defaults for these parameters.

Each dip computation is independently processed; no vertical continuity requirement or clustering routine is employed in MSD computations. Because each computed dip is therefore independent of other dips, successive dip computations that agree closely are more likely to reflect the actual dip within the formation. Each computed dip is assigned an empirical quality factor ranging from a low of 0 to a high of 20. This factor is a function of the number of iterations made when seeking the best-fit plane, and is also one of several conditions that determine selection of the final plane. The factor is then shown qualitatively on the final dip plots as an interpretation aid.

Dips picked by parameterized dipmeter processing are presented on a dip vs. depth plot, with the azimuth of dip direction indicated by a tick on the dip symbol. When the plot is generated, dip quality thresholds are specified that determine whether a given dip computation will be included on the plot and if included, whether the dip will be represented as one of higher or lower quality. This type of plot is often presented together with caliper or resistivity curves, and with an indication of the dip and azimuth of borehole drift (deviation from the vertical).

Commonly, dips are plotted at a depth slightly offset from the depth that might appear to be the ideal interval for dip computations on the FMS images. The reason for this is that the eye recognizes mainly the border between light and dark on the gray-scale image, whereas the dipmeter computations correlate primarily waveforms that may not necessarily correspond to the light-to-dark image that the eye sees. The locations and frequency of MSD dipmeter computations are determined by the processing parameters. Because dipmeter computations are made against a range of resistivity values with much higher resolution than the gray scale in which the plotted FMS image is presented, this offset is not a problem unless the computed dip differs greatly from the dip suggested by features visible in the gray-scale image.

Dipmeter computations and manually determined structural measurements for the same hole region can differ significantly. Several reasons for this disparity may be postulated. A major consideration is the precision of the manually determined structural measurements. Manually derived dips are recalculated from two orthogonal apparent dips on a small core (see "Structural Geology" section, this chapter), which are averaged from bedding surfaces that are commonly erosive and are thus rarely perfectly planar or necessarily representative of bedding on a larger scale. Furthermore, in near-horizontal strata an error of 1° in the measurement of an apparent dip can potentially be magnified into a much larger error, particularly in the direction of dip. For dips of less than 5° the error in the reconstructed azimuth may be in excess of ±15° (see "Structural Geology" section). For steeper dips, for example, in strata dipping 10°–15°, this calculation error is reduced to approximately ±2° of true dip and ±5° of strike only. Errors are also likely to be introduced during reorientation, as the precision of the multishot tool and paleomagnetic declination values are each estimated to be in the order of ±3°.

The limitations of dipmeter measurements should also be emphasized. Although the analysis software is designed to minimize spurious correlations, it is nevertheless a straightforward algorithm lacking human judgement or relevant external information, although the algorithm is optimized for the well-bedded clastic sequences usually encountered in or around petroleum reservoirs. Erroneous dip computations are inevitable as they are caused by signatures in the microresistivity curves that meet the dipmeter correlation requirements but are the result of factors other than formation dip. An example of a feature that would lead to an erroneous MSD dip computation is a mud-clast conglomerate interval that contains rounded clasts that could be many tens of centimeters or even a few meters in diameter. The intersection of these clasts with the borehole wall will generate what appears to be bedding, but with random orientation. Whereas the structural geologist making dip measurements is manually looking at the core and is able to avoid making measurements in such areas, the automatic dip computation routine does not have this outside core-based information and can make a dip computation where it is inappropriate.

Another factor that could lead to complications of FMS analysis is the deformation of the borehole wall and formation geometry by drilling. This might be expected to be most significant adjacent to washouts and at the boundaries between lithologies of differing competence, for example, between nannofossil oozes and volcaniclastic turbidite horizons. Recognizable, drilling-induced disturbance of bed dip in the core is accounted for when manual dip measurements are made (see "Structural Geology"), but cannot be excluded from the dipmeter data. Therefore, interpretations of the dipmeter plots should be made carefully, with an awareness of the nature of dipmeter computation algorithms, and in conjunction with detailed lithostratigraphic information. Ideally, conclusions should be made from clusters of similarly oriented dip symbols rather than from individual measurements.

General Purpose Inclinometer Tool

The general purpose inclinometer tool (GPIT) provides a measurement of borehole inclination, the orientation of the tool with respect to the Earth's magnetic field using a three-component magnetometer, and tool motion using an accelerometer. It is run with the FMS to provide spatial orientation of the borehole wall images.

Borehole Televiewer

The borehole televiewer (BHTV) produces an ultrasonic acoustical image of the borehole wall. A transducer emits ultrasonic pulses at a frequency of 1.3 MHz, which are reflected at the borehole wall and then received by the same transducer. The amplitude and traveltime of the reflected signal are determined and recorded either as analog signals (analog BHTV) or stored in the logging computer (digital BHTV). The continuous rotation of the transducer and upward motion of the tool produce a complete map of the borehole wall.

The amplitude depends on the reflection coefficient of the borehole fluid/rock interface, the position of the BHTV tool in the borehole, the shape of the borehole, and the roughness of the borehole wall. The change in roughness of the borehole wall (e.g., at fractures intersecting the borehole) is responsible for the modulation of the reflected signal; therefore, fractures or changes in the character of the drilled rocks can easily be recognized in the amplitude image. On the other hand, the recorded traveltime image gives detailed information about the shape of the borehole: knowing the velocity of the ultrasonic signal in the borehole fluid allows calculation of one caliper value of the borehole from each recorded traveltime. As 128 points are typically recorded per transducer revolution, the BHTV can be regarded, in effect, as a "multiarm caliper log." Amplitude and traveltime are recorded together with a reference to magnetic north by means of a magnetometer, permitting the orientation of data.

The images can be used to reorient cores, if the cores have features (e.g., inclined bedding) that can be recognized in the BHTV data. The BHTV can also be used to measure stress in the borehole through the delineation of breakouts. In an isotropic, linearly elastic rock subjected to an anisotropic stress field, breakouts form in the direction of the axis of least principal horizontal stress. On Leg 135, the digital BHTV was unavailable because of electronic failure; the analog BHTV tool was deployed instead. However, problems encountered during recording rendered the entire data set unusable.

Lamont-Doherty Temperature Tool

The Lamont-Doherty temperature tool is a self-contained tool that can be attached to any Schlumberger tool string. Data from two thermistors (one taking measurements once every second and the other once every 5 s) and a pressure transducer (sampling every 5 s) are collected and stored in a Tattletale computer within the tool. Following the logging run, the data are dumped from the Tattletale to the Masscomp computer for analysis. A fast-response, but relatively low-accuracy, thermistor is able to detect sudden, very small temperature excursions caused by fluid flow from the formation. A slow-response, high-accuracy thermistor can be used to estimate heat flow if one knows the history of drilling-fluid circulation in the hole and if one has at least two temperature logs (Jaeger, 1961). Data are recorded as a function of time; conversion to depth can be based on the pressure transducer or, preferably, on simultaneous recording by Schlumberger logs of an elapsed time curve and depth curve.

Log Data Quality

The quality of the log data may be seriously degraded in excessively wide sections of the borehole, by high wall rugosity, or by rapid changes in the hole diameter. Resistivity and velocity measurements are less sensitive to changes in borehole size than the nuclear measurements (density, neutron porosity, and both natural and induced spectral gamma ray). The latter are seriously impaired because of the large signal attenuation by the borehole fluid. Corrections can be applied to the original data to reduce the effects of these conditions and, generally, any departure from the conditions under which the tool was calibrated.

Different logs may have small depth mismatches, caused by either stretching of the cable or heaving of the ship during recording. Small errors in depth matching can impair the results in zones of rapidly varying lithology. To minimize such errors, a hydraulic heave compensator adjusts for rig motion. Precise depth matching of logs with cores is not possible in zones where core recovery is low because of the inherent ambiguity of placing the recovered section within the interval cored.

Log Analysis

During logging, incoming data are observed in real time on a monitor oscilloscope and simultaneously recorded on digital tape in the Schlumberger logging unit. After logging, these tapes are read by the Masscomp computer system or the VAXstation 3200 in the downhole measurements laboratory and reformatted to a file format compatible with the Terralog log-interpretation software package. Terralog is an interactive system that permits many log manipulation and plot options.

The log analysis and interpretation varies in duration and procedure for each site. Most of the log processing is conducted aboard ship; further analysis and interpretation are done after the cruise, using a companion system in the Borehole Research Laboratory of Lamont-Doherty Geological Observatory.

Reprocessing of Logs

Sonic logs obtained in real time are not based on full-waveform analysis, but on a thresholding technique that attempts to detect the compressional wave arrival by a first-break criterion. Occasionally this technique fails and either the threshold is exceeded by noise or the first compressional arrival is below the threshold. This phenomenon, called cycle skipping, creates spurious spikes on the sonic log. On Leg 135, raw traveltimes were reprocessed when necessary with an algorithm designed to reject cycle skips (Srivastava, Arthur, et al., 1987).

Raw geochemical logs for Leg 135 are shown following the barrel sheets for each site at which the geochemical tool string was run. Raw count rates for six elements (Ca, Si, Fe, S, Cl, and H) are obtained in real time by the Schlumberger data acquisition software. Post-cruise reprocessing uses a Schlumberger Elite 1000 workstation and proprietary Schlumberger software. The gamma spectrum at each depth is inverted for titanium, gadolinium, and potassium in addition to the six elements in the shipboard inversion. Though gadolinium is present in concentrations that rarely exceed a few parts per million, its neutron capture cross section is so large that it can account for 10%–30% of the total gamma spectrum. Inclusion of these additional elements improves the quality of the overall inversion, particularly improving the accuracy of the calculated calcium abundance, by converting sources of unaccounted variance to signals. Aluminum concentrations from the ACT are adjusted for variations in cable speed. Changes in logging speed affect the time lag between neutron irradiation of the formation and recording of the induced gamma spectrum, because the number of induced gamma rays decreases rapidly with time. However, the small amount of ship heave during logging may make this correction less reliable in ODP holes than in land wells.

When the lithodensity tool is also run at the same site where the geochemical tool string is run, further reprocessing of geochemical logs is possible. The relative abundances of Ca, Si, Fe, Ti, Al, K, S, Th, U, and Gd are used to calculate a log of predicted photoelectric effect. The difference between this log and the actual log of photoelectric effect can be attributed to the only two major elements not directly measured, Mg and Na. Major ele-

ments are expressed in terms of oxide dry-weight percent, based on the assumption that oxygen is 50% of the total dry weight.

REFERENCES

American Society of Testing and Materials, 1989. *Annual Book of ASTM Standards for Soil and Rock; Building Stones:* Geotextiles (Vol. 04.08): Philadelphia (ASTM), 168–862.

Archie, G. E., 1942. The electrical resistivity log as an aid in determining some reservoir characteristics. *J. Pet. Tech.*, 5:1–8.

Berggren, W. A., Kent, D. V., Flynn, J. J., and Van Couvering, J. A., 1985a. Cenozoic geochronology. *Geol. Soc. Am. Bull.*, 96:1407–1418.

Berggren, W. A., Kent, D. V., and Van Couvering, J. A., 1985b. The Neogene: Part 2. Neogene geochronology and chronostratigraphy. *In* Snelling, N. J. (Ed.), *The Chronology of the Geological Record.* Geol. Soc. London Mem., 10:211–260.

Bernard, B. B., Brooks, J. M., and Sackett, W. M., 1976. Natural gas seepage in the Gulf of Mexico. *Earth Planet. Sci. Lett.*, 31:48–54.

_____, 1978. Light hydrocarbons in recent Texas continental shelf and slope sediments. *J. Geophys. Res.*, 83:4053–4061.

Blanc, G., Boulegue, J., Badaut, D., and Stouff, P., 1986. Premiers résultats de la campagne océanographique Hydrotherm du Marion Dufresne sur la fosse Atlantis II. *C. R. Acad. Sci. Ser. 2*, 302:175–180.

Blanc, G., Boulegue, J., and Charlou, J. L., 1990. Light hydrocarbon profiles in the sea water, brines, and metalliferous sediment interstitial waters of the Atlantis II Deep (Red Sea). *Oceanol. Acta*, 13:187–197.

Blow, W. H., 1969. Late middle Eocene to Recent planktonic foraminiferal biostratigraphy. *In* Brönniman, P., and Renz, H. H. (Eds.), *Proc. First Int. Conf. Planktonic Microfossils*, Geneva, 1967. Leiden (E. J. Brill), 1:199–422.

Boyce, R. E., 1973. Appendix I. Physical properties—methods. *In* Edgar, N. T., Saunders, J. B., et al., *Init. Repts. DSDP*, 15: Washington (U.S. Govt. Printing Office), 1115–1128.

_____, 1976. Definitions and laboratory techniques of compressional sound velocity parameters and wet-water content, wet-bulk density, and porosity parameters by gravimetric and gamma ray attenuation techniques. *In* Schlanger, S. O., Jackson, E. D., et al., *Init. Repts. DSDP*, 33: Washington (U.S. Govt. Printing Office), 931–958.

_____, 1977. Deep Sea Drilling Project procedures for shear strength measurement of clayey sediment using modified Wykeham Farrance laboratory vane apparatus. *In* Barker, P., Dalziel, I.W.D., et al., *Init. Repts. DSDP*, 36: Washington (U.S. Govt. Printing Office), 1059–1068.

Bryan, W. B., 1972. Morphology of quench crystals in submarine basalts. *J. Geophys. Res.*, 77:5812–5819.

Bukry, D., 1973. Low-latitude coccolith biostratigraphic zonation. *In* Edgar, N. T., Saunders, J. B., et al., *Init. Repts. DSDP*, 15: Washington (U.S. Govt. Printing Office), 685–703.

_____, 1975. Coccolith and silicoflagellate stratigraphy, northwestern Pacific Ocean, Deep Sea Drilling Project Leg 32. *In* Larson, R. L., Moberly, R., et al., *Init. Repts. DSDP*, 32: Washington (U.S. Govt. Printing Office), 677–701.

Chaproniere, G.C.H., 1981. Australasian mid-tertiary larger foraminiferal associations and their bearing on the East Indian letter classification. *Bur. Miner. Resour., Geol. Geophys. (Aust.)*, 6:145–151.

_____, 1983. Tertiary larger foraminiferids from the northwestern margin of the Queensland Plateau, Australia. *Bur. Miner. Resour., Geol. Geophys. (Aust.)*, 217:31–57.

_____, in press. Pleistocene to Holocene planktic foraminiferal biostratigraphy of the Coral Sea, offshore Queensland, Australia. *BMR J. Aust. Geol. Geophys.*

Clement, B. M., and Robinson, F., 1987. The magnetostratigraphy of Leg 94 sediments. *In* Ruddiman, W. F., Kidd, R. B., Thomas, E., et al., *Init. Repts. DSDP*, 94, Pt. 2: Washington (U.S. Govt. Printing Office), 635–650.

Dewen, J. T., 1983. *Essentials of Modern Open Hole Log Interpretations:* Tulsa (PennWell).

Dowsett, H. J., 1989. Application of the graphic correlation method to Pliocene marine sequences. *Mar. Micropaleontol.*, 14:3–32.

Dunham, R., 1962. Classification of carbonate rocks according to depositional texture. *In* Ham, W. E. (Ed.), *Classification of Carbonate Rocks.* AAPG, 108–121.

Embry, A. F., and Klovan, E. J., 1971. A late Devonian reef tract on northeastern Banks Island, Northwest Territories. *Bull. Can. Pet. Geol.*, 19:730–781.

Emeis, K.-C., and Kvenvolden, K. A., 1986. Shipboard organic geochemistry on *JOIDES Resolution. ODP Tech. Note*, No. 7.

Espitalié, J., Deroo, G., and Marquis, F., 1985a. La pyrolyse Rock-Eval et ses applications. *Rev. Inst. Fr. Pet.*, 40:563–579.

_____, 1985b. La pyrolyse Rock-Eval et ses applications. *Rev. Inst. Fr. Pet.*, 40:755–784.

_____, 1986. La pyrolyse Rock-Eval et ses applications. *Rev. Inst. Fr. Pet.*, 41:73–89.

Fisher, R. V., and Schmincke, H.-U., 1984. *Pyroclastic Rocks:* New York (Springer-Verlag).

Gieskes, J. M., 1973. Interstitial water studies, Leg 15: alkalinity, pH, Mg, Ca, Si, PO_4, and NH_4. *In* Heezen, B. C., MacGregor, I. D., et al., *Init. Repts. DSDP*, 20: Washington (U.S. Govt. Printing Office), 813–829.

Gieskes, J. M., and Peretsman, G., 1986. Water chemistry procedures aboard *JOIDES Resolution*—some comments. *ODP Tech. Note*, No. 5.

Harland, W. B., Cox, A. V., Llewellyn, P. G., Pickton, C.A.G., Smith, D. G., and Walters, R., 1982. *A Geologic Time Scale:* Cambridge (Cambridge Univ. Press).

Hertzog, R., 1979. Laboratory and field evaluation of an inelastic-neutron-scattering and capture gamma-ray spectroscopy tool. *Soc. Pet. Eng. Pap.*, No. 7430.

Hyndman, R. D., Langseth, M. G., and Von Herzen, R. P., 1987. Deep Sea Drilling Project geothermal measurements: a review. *Rev. Geophys.*, 25:1563–1582.

Jaeger, J. C., 1961. The effect of the drilling fluid on temperatures measured in boreholes. *J. Geophys. Res.*, 66:563–569.

Kennett, J. P., and Srinivasan, M. S., 1983. *Neogene Planktonic Foraminifera: A Phylogenetic Atlas:* Stroudsburg, PA (Hutchinson Ross).

Lee, H. J., 1984. State of the art: laboratory determination of strength of marine soils. *In* Chaney, R. C., and Demars, K. R. (Eds.), *Strength Testing of Marine Sediments: Laboratory and In-Situ Measurements:* ASTM Spec. Tech. Publ., 883:181–250.

Manheim, F. T., and Sayles, F. L., 1974. Composition and origin of interstitial waters of marine sediments based on deep sea drill cores. *In* Goldberg, E. D. (Ed.), *The Sea* (Vol. 5): New York (Wiley), 527–568.

Martini, E., 1971. Standard Tertiary and Quaternary calcareous nannoplankton zonation. *In* Farinacci, A. (Ed.), *Proc. 2nd Planktonic Conf. Roma:* Rome (Ed. Technosci.), 2:739–785.

Matthews, D. J., 1939. *Tables of the Velocity of Sound in Pure Water and Seawater for Use in Echo-sounding and Sound-ranging:* London (Hydrographic Dept. Admiralty).

Mazzullo, J. M., Meyer, A., and Kidd, R., 1987. New sediment classification scheme for the Ocean Drilling Program. *In* Mazzullo, J., and Graham, A. G. (Eds.), *Handbook for Shipboard Sedimentologists.* ODP Tech. Note, 8:45–67.

McKee, E. D., and Weir, G. W., 1953. Terminology for stratification and cross-stratification in sedimentary rocks. *Geol. Soc. Am. Bull.*, 64:381–390.

Moore, J. C., Mascle, A., et al., 1990. *Proc. ODP, Sci. Results*, 110: College Station, TX (Ocean Drilling Program).

Munsell Soil Color Charts, 1975. Baltimore (Kollmonger Corp.).

Natland, J. H., 1978. Crystal morphologies in basalts from DSDP Site 395, 23°N, 46°W, Mid-Atlantic Ridge. *In* Melson, W. G., Rabinowitz, P. D., et al., *Init. Repts. DSDP*, 45: Washington (U.S. Govt. Printing Office), 423–445.

Norrish, K., and Hutton, J. T., 1969. An accurate X-ray spectrographic method for the analysis of a wide range of geological samples. *Geochim. Cosmochim. Acta.*, 33:431–453.

Okada, H., and Bukry, D., 1980. Supplementary modification and introduction of code numbers to the low-latitude coccolith biostratigraphic zonation (Bukry, 1973; 1975). *Mar. Micropaleontol.*, 5:321–325.

Reynolds, R. C., 1967. Estimations of mass absorption coefficients by Compton scattering: improvements and extensions of the method. *Am. Mineral.*, 48:1133–1143.

Schlumberger, 1986. *Dipmeter Interpretation Fundamentals:* New York (Schlumberger).

_____, 1989. *Log Interpretation Principles/Applications:* Houston (Schlumberger Educational Services).
Serra, O., 1984. *Fundamentals of Well Log Interpretation: The Acquisition of Logging Data:* Amsterdam (Elsevier).
_____, 1989. *Formation MicroScanner Image Interpretation:* Houston (Schlumberger Educational Services).
Shepard, F., 1954. Nomenclature based on sand-silt-clay ratios. *J. Sediment. Petrol.*, 24:151–158.
Shipboard Scientific Party, in press. Introduction and Explanatory Notes. *In* Taira, A., Hill, I., Firth, J., et al., *Proc. ODP, Init. Repts.*, 131: College Station, TX (Ocean Drilling Program).
Srivastava, S. P., Arthur, M., Clement, B., et al., 1987. *Proc. ODP, Init. Repts.*, 105: College Station, TX (Ocean Drilling Program).
Timur, A., and Toksöz, M. N., 1985. Fundamentals of well log interpretation. *Annu. Rev. Earth Planet. Sci.*, 13:315–344.
Vacquier, V., 1985. The measurement of thermal conductivity of solids with a transient linear heat source on the plane surface of a poorly conducting body. *Earth Planet. Sci. Lett.*, 74:275–279.
Von Herzen, R. P., and Maxwell, A. E., 1959. The measurement of thermal conductivity of deep-sea sediments by a needle probe method. *J. Geophys. Res.*, 65:1557–1563.
Wentworth, C. K., 1922. A scale of grade and class terms for clastic sediments. *J. Geol.*, 30:377–392.
Yokota, I., Kinoshita, K., and Uyeda, S., 1979. New DSDP (Deep Sea Drilling Project) downhole temperature probe utilizing digital self-recording system with IC RAM elements. *Bull. Earthq. Res. Inst. Univ. Tokyo,* 54:441–462.

Ms 135A-102